



HAL
open science

Sir3 heterochromatin protein promotes non-homologous end joining by direct inhibition of Sae2

Hélène Bordelet, Rafaël Costa, Clémentine Brocas, Jordane Dépagne, Xavier Veaute, Didier Busso, Amandine Batté, Raphaël Guérois, Stéphane Marcand, Karine Dubrana

► To cite this version:

Hélène Bordelet, Rafaël Costa, Clémentine Brocas, Jordane Dépagne, Xavier Veaute, et al.. Sir3 heterochromatin protein promotes non-homologous end joining by direct inhibition of Sae2. *EMBO Journal*, 2021, 41, pp.e108813. 10.15252/embj.2021108813 . hal-04312115

HAL Id: hal-04312115

<https://hal.science/hal-04312115>

Submitted on 19 Jan 2024

HAL is a multi-disciplinary open access archive for the deposit and dissemination of scientific research documents, whether they are published or not. The documents may come from teaching and research institutions in France or abroad, or from public or private research centers.

L'archive ouverte pluridisciplinaire **HAL**, est destinée au dépôt et à la diffusion de documents scientifiques de niveau recherche, publiés ou non, émanant des établissements d'enseignement et de recherche français ou étrangers, des laboratoires publics ou privés.

Sir3 Heterochromatin Protein Promotes NHEJ by Direct Inhibition of Sae2

Hélène Bordelet^{1,2}, Rafaël Costa¹, Clémentine Brocas¹, Jordane Dépagne³, Xavier Veaute³, Didier Busso³, Amandine Batté^{1,4}, Raphaël Guérois⁵, Stéphane Marcand¹ and Karine Dubrana^{1*}

1. Université de Paris and Université Paris-Saclay, INSERM, iRCM/IBFJ CEA, UMR Stabilité Génétique Cellules Souches et Radiations, F-92265, Fontenay-aux-Roses, France.

2. Régulation spatiale des génomes, Institut Pasteur, CNRS UMR3525, 75015 Paris, France

3. CIGEx platform. Université de Paris and Université Paris-Saclay, INSERM, iRCM/IBFJ CEA, UMR Stabilité Génétique Cellules Souches et Radiations, F-92265, Fontenay-aux-Roses, France.

4. Center for Integrative Genomics, Bâtiment Génopode, University of Lausanne, Lausanne, Switzerland.

5. Institute for Integrative Biology of the Cell (I2BC), CEA, CNRS, Université Paris-Sud, Université Paris-Saclay, Gif-sur-Yvette, France

* Corresponding author: karine.dubrana@cea.fr

1 **Abstract**

2 Heterochromatin is a conserved feature of eukaryotic chromosomes, with
3 central roles in gene expression regulation and maintenance of genome stability.
4 How **heterochromatin proteins regulate DNA repair** remains poorly described. In
5 *Saccharomyces cerevisiae*, the Silent Information Regulator (SIR) complex
6 assembles heterochromatin-like chromatin at subtelomeres. SIR-mediated repressive
7 chromatin limits double strand break (DSB) resection protecting damaged
8 chromosome ends during HR. As resection initiation marks the cross-road between
9 repair by non-homologous end joining (NHEJ) or HR, we asked whether SIR-
10 mediated heterochromatin regulates NHEJ. We show that SIRs promote NHEJ
11 through two pathways, one depending on repressive chromatin assembly, and the
12 other relying on Sir3 in a manner that is independent of its heterochromatin-
13 promoting function. Sir3 physically interacts with Sae2 and this interaction impairs
14 **Sae2-dependent MRX functions**. As a consequence, Sir3 limits Mre11-mediated
15 resection, delays MRX removal from DSB ends and promotes NHEJ.

1 **Main Text:**

2 **Introduction**

3

4 DNA double strand breaks (DSBs) are genotoxic lesions typically repaired by two
5 conserved repair pathways: Non-Homologous End Joining (NHEJ) and Homologous
6 Recombination (HR). NHEJ ligates DSB ends with minimal or no processing, and acts
7 throughout the cell cycle. Repair by HR requires a homologous template for repair, the
8 resection of the DSB ends, and occurs in S and G2 phases. Initiation of DSB resection thus
9 represents a decision point between NHEJ and HR, upon which various cellular inputs
10 converge.

11 DSB ends are rapidly bound by the Ku70/80 and Mre11-Rad50-Xrs2^{NBS1} (MRX^{MRN})
12 end binding complexes. In *S. cerevisiae*, both complexes aid recruitment of the NHEJ ligation
13 complex composed of the yeast DNA ligase IV Dnl4 (Lig4) and its XRCC4/XLF-like
14 regulatory subunits Lif1 and Nej1 (Palmbos et al. 2005, 2008; Matsuzaki et al. 2008; Chen
15 and Tomkinson 2011; Mahaney et al. 2014).

16 In addition to its function in NHEJ, the MRX^{MRN} complex is key to shifting repair
17 towards HR when stimulated to initiate resection by Sae2. Indeed, Sae2 activates the
18 endonuclease activity of MRX^{MRN}, which cleaves the 5' strand of the DSB end (Cannavo and
19 Cejka 2014; Bazzano et al. 2021). This provides an entry point for MRX 3'-5' exonuclease
20 activity, which degrades the DNA towards the DSB, creating a short ssDNA extensions that
21 can no longer be ligated by the canonical NHEJ machinery (Mimitou and Symington 2008;
22 Garcia et al. 2011; Cannavo and Cejka 2014). Impairment of Sae2-MRX dependent
23 resection increases error-prone NHEJ, highlighting the role of Sae2 in coordinating DSB
24 repair pathway choice (Lee and Lee 2007; Huertas et al. 2008).

25 As a key determinant of NHEJ/HR repair balance, Sae2 activity and protein levels are
26 tightly regulated. Sae2 activity is cell cycle regulated and restricted to S-G2 by CDK-
27 dependent phosphorylation (Huertas et al. 2008). Upon DNA damage, the Tel1 and Mec1
28 checkpoint kinases phosphorylate Sae2, altering its oligomerization state and forming units
29 active for repair (Baroni et al. 2004; Fu et al. 2014). Sae2 is also negatively regulated by
30 acetylation, which favours its degradation by autophagy thus preventing the persistence of
31 active Sae2 in the cell (Robert et al. 2011; Fu et al. 2014).

32 In cells, DSB repair does not occur on naked DNA, but in the context of chromatin,
33 which modulates repair efficiency and outcome in several organisms (Goodarzi et al. 2008;
34 Chiolo et al. 2011; Lemaître et al. 2014; Tsouroula et al. 2016; Batté et al. 2017). In *S.*
35 *cerevisiae* haploid cells, heterochromatin-like chromatin (also called silent chromatin)
36 establishes at the two cryptic mating type loci (*HM* loci) and at each of the 32 subtelomeric
37 loci. Its core components are histone H4 lysine 16 deacetylated nucleosomes, which are

38 bridged by the histone-binding factor Sir3 in complex with the protein Sir4 and the histone
39 deacetylase Sir2 (Behrouzi et al. 2016; Gartenberg and Smith 2016; Faure et al. 2019). Sir2
40 deacetylates histone H4 lysine 16 thus promoting Sir3 binding and propagation along
41 chromatin. The limiting factor of heterochromatin propagation is Sir3, and its overexpression
42 is sufficient to increase silent chromatin spreading and transcriptional repression in
43 subtelomeric regions, providing an ideal genetic tool to modulate silent chromatin at given
44 sites (Renauld et al. 1993; Hecht et al. 1996; Strahl-Bolsinger et al. 1997; Katan-Khaykovich
45 and Struhl 2005). Sir3 can be seen as the functional ortholog of the heterochromatin factor
46 HP1 that binds histones H3 methylated on lysine 9 in other eukaryotes (Larson et al. 2017;
47 Strom et al. 2017; Machida et al. 2018; Allshire and Madhani 2018). In addition, general
48 heterochromatin properties are conserved in budding yeast such as *cis* and *trans*
49 cooperativity in the establishment of transcription repressive compartments, clustering at the
50 nuclear periphery and near the nucleolus, epigenetic variegation and late replication initiation
51 (Meister and Taddei 2013; Ruault et al. 2021).

52 SIR proteins also contribute to genome stability in several ways. Sir4 inhibits telomere
53 end fusions by NHEJ (Marcand et al. 2008) and favours telomere elongation through
54 telomerase recruitment (Dalby et al. 2013; Hass and Zappulla 2015; Chen et al. 2018).
55 However, the SIR complex also indirectly promotes NHEJ, as derepression of the *HM* loci in
56 *sir* mutants and the resulting expression of the $\alpha 1$ - $\alpha 2$ repressor inhibits NHEJ through
57 negative transcriptional regulation of Nej1, and to a lesser extent Lif1 (Aström et al. 1999;
58 Lee et al. 1999; Kegel et al. 2001; Frank-Vaillant and Marcand 2001; Valencia et al. 2001).
59 Finally, we recently showed that SIR-mediated heterochromatin structure protects
60 subtelomeric DSBs from extensive resection (Batté et al. 2017). Whether SIR proteins also
61 inhibit resection initiation and as such play a direct NHEJ-promoting role at subtelomeres is
62 unknown.

63 Here we found that Sir3 promotes NHEJ in *cis* through heterochromatin formation, as
64 well as in *trans* independently of heterochromatin formation. The *trans* effect relies on a
65 direct interaction between Sir3 and Sae2 that regulates NHEJ repair. This interaction,
66 between the Sir3 conserved AAA+ domain and the C-terminal domain of Sae2, inhibits Sae2
67 functions. Sae2-Sir3 interaction limits Sae2-MRX dependent resection and favours NHEJ.
68 This function is separable from Sir3-mediated heterochromatin assembly, revealing a new
69 role for SIRs in regulating DSB repair. Sir3 not only promotes genome stability as part of
70 heterochromatin, but is also a direct negative regulator of Sae2, and thus a pro-NHEJ repair
71 factor.

72

73 **Results**

74 **NHEJ is increased in *cis* and in *trans* by Sir3 overexpression**

75 Yeast heterochromatin (Sir3-mediated silent chromatin) delays DSB resection,
76 favouring accurate repair by HR near chromosome ends (Batté et al. 2017). Nevertheless,
77 heterochromatin impact on NHEJ has not been addressed. To explore this issue, we used
78 erroneous NHEJ repair of an I-SceI-induced DSB as a proxy for NHEJ efficiency. To
79 establish heterochromatin at the I-SceI site, we exploited the ability of Sir3 overexpression to
80 spread heterochromatin specifically along subtelomeric regions (Batté et al. 2017). The I-
81 SceI site inserted at a subtelomere (1.4 kb from *TEL6R*) is embedded in euchromatin in wild-
82 type (WT) cells but assembled in heterochromatin in cells overexpressing Sir3. Conversely,
83 the I-SceI site inserted at an intrachromosomal position (*LYS2* locus, 300 kb from the closest
84 telomere) remains euchromatic in both contexts (Hocher et al. 2018). Continuous I-SceI
85 expression, driven by a galactose-inducible promoter, is lethal unless NHEJ repairs the DSB
86 with a sequence change that prevents a new cleavage by I-SceI (Fig 1A). Survival frequency
87 was around 10^{-3} in WT cells, and was reduced 10-fold in cells lacking Ligase 4 (Dnl4),
88 indicating that most events leading to survival were products of classical NHEJ (Fig 1B, 1C).

89 Sir3 overexpression led to a 25-fold increase in survival after DSB induction at *TEL6R*
90 which was mainly Dnl4-dependent (Fig 1B). DNA sequencing of repair junctions confirmed
91 that Sir3 overexpression led to increased NHEJ in subtelomeres (Fig 1B and EV1). This
92 effect partly relied on heterochromatin formation since in the absence of Sir4, the NHEJ
93 increase caused by Sir3 overexpression was less pronounced (Fig 1B). However, NHEJ
94 levels in *sir4Δ* cells overexpressing Sir3 remained 7-fold higher than in WT cells, suggesting
95 that Sir3 overexpression also increased NHEJ independently of heterochromatin formation.
96 Consistently, Sir3 overexpression increased NHEJ levels at a euchromatic DSB, although to
97 a more modest extent (Fig 1C, EV1). This data suggests that heterochromatin favours NHEJ
98 repair, and that an excess of Sir3 also stimulates NHEJ in *trans* independently of
99 heterochromatin assembly.

100 **Sir3 overexpression inhibits MRX-Sae2**

101 Increased NHEJ is a typical phenotype of impaired Mre11 nuclease activity as
102 observed in the *mre11-H125N* nuclease deficient mutant or in absence of its regulator Sae2
103 (Lee and Lee 2007; Huertas et al. 2008; Huertas and Jackson 2009). Consistently, the
104 absence of *SAE2* and the *mre11-H125N* point mutation led to an epistatic 8-fold increase in
105 NHEJ at euchromatic *TEL6R* and *LYS2* DSB sites (Fig 1B and 1C). We thus tested if Sir3-
106 mediated heterochromatin and the *trans* effect of Sir3 overexpression on NHEJ could result
107 from a defect in Mre11 nuclease activity.

108 At heterochromatic DSB sites, the deletion of *SAE2* in cells overexpressing Sir3 did
109 not further increase NHEJ, suggesting that MRX-Sae2 is inhibited (Fig 1B). However, *SAE2*
110 deficiency by itself had a significantly lower effect than Sir3 overexpression, indicating that

111 heterochromatin favours NHEJ beyond MRX-Sae2 inhibition. At the euchromatic *LYS2* site,
112 *SAE2* deletion or *mre11-H125N* mutation increased NHEJ in an epistatic manner and to the
113 same extent as Sir3 overexpression (Fig 1C). NHEJ frequencies were not further increased
114 in *sae2Δ* cells overexpressing Sir3 suggesting that Sae2 and Mre11 nuclease activity are
115 inhibited in these cells. Altogether, these results argue that heterochromatin favours NHEJ
116 repair and that the overexpression of Sir3 inhibits MRX-Sae2 in *trans*.

117 The MRX-Sae2 complex is important to initiate resection of DSB ends (Mimitou and
118 Symington 2008; Garcia et al. 2011; Cannavo and Cejka 2014). To confirm the *trans*
119 inhibition of MRX-Sae2, we tested if Sir3 overexpression could delay resection at a
120 euchromatic site. To assess DSB resection, we employed a PCR-based method to evaluate
121 the resection kinetics at 0.2 and 1 kb from the I-SceI cutting site (Fig 1D and EV1; (Batté
122 et al. 2017)). Sir3 overexpression delayed resection of the euchromatic DSB after galactose
123 addition, mimicking the resection delay observed in *sae2Δ* cells (Fig 1E and EV1). The
124 resection delays conferred by *SAE2* deletion and Sir3 overexpression were epistatic (Fig 1E
125 and EV1), consistent with an inhibition of the nuclease activity of the MRX-Sae2 complex
126 upon Sir3 overexpression.

127 Increased persistence of Mre11 at DSB is typically observed when Mre11 nuclease
128 activity is altered, as seen in *mre11-H125N* mutant or in *SAE2* deficient cells (Lisby and
129 Rothstein 2004; Clerici et al. 2006; Cannavo and Cejka 2014; Yu et al. 2018). In agreement
130 with an inhibition of MRX-Sae2 by Sir3, cells overexpressing Sir3 accumulated Mre11 foci
131 following DSB induction (Fig 1F, 1G). The increase in Mre11 foci was comparable to that
132 observed in *sae2Δ* mutants and was not increased upon additional Sir3 overexpression (Fig
133 1G). Thus, overexpression of Sir3 affects Mre11 turnover at euchromatic DSB sites,
134 recapitulating another typical phenotype of impaired Mre11 nuclease activity. To conclude,
135 Sir3 overexpression increases NHEJ at subtelomeric DSBs through at least two pathways.
136 One that relies on its ability to assemble heterochromatin, and another that limits MRX-Sae2
137 activity but is independent of heterochromatin formation.

138 **Sir3 inhibits Sae2 in a dose dependent manner**

139 To dissect the mechanism underlying the inhibition of MRX-Sae2 following Sir3
140 overexpression, we tested whether this effect was modulated by Sir3 dosage. Under the
141 control of the strong *pGPD* promoter, Sir3 expression increases 29-fold compared to WT. In
142 contrast, under the weaker *pADH1* promoter, Sir3 expression increases only 9-fold (Hocher
143 et al. 2018). We observed that lower Sir3 overexpression resulted in a lesser increase in
144 NHEJ, indicating that Sir3 overexpression impacts NHEJ in a dose dependent manner (Fig
145 1H).

146 Upon Sir3 overexpression, Mre11 recruitment to DSB was maintained (Fig 1F), but
147 resection was delayed (Fig 1E), suggesting that Sae2, rather than Mre11, might be the target
148 of Sir3. If true, Sir3 dependent NHEJ increase should be suppressed by Sae2 co-
149 overexpression. To perform Sae2 overexpression, we transformed cells with a high-copy
150 number plasmid bearing the *SAE2* gene under the control of its own promoter. Sae2
151 overexpression lowers NHEJ levels in *sae2Δ* cells, showing that overexpressed-Sae2 is
152 functional (Fig 1H). Sae2 overexpression partially suppressed the effect of very high Sir3
153 levels (*pGPD* promoter, 2 μ *SAE2*) and completely suppressed the effect of moderately high
154 Sir3 levels (*pADH1* promoter, 2 μ *SAE2*) (Fig 1H). Thus, increased Sae2 expression
155 counteracts the effects of Sir3 overexpression on NHEJ, indicating that Sir3 regulates Sae2
156 levels or activity.

157 **Sae2 and Sir3 interact *in vivo* and *in vitro***

158 Since Sae2 is limiting for normal resection rate (Robert et al. 2011; Tsabar et al.
159 2015), we addressed the possibility that Sir3 overexpression could regulate cellular levels of
160 Sae2. To do so, GFP fused *SAE2* protein levels were quantified by Western blot in WT or
161 Sir3 overexpressing cells. We observed no major difference in Sae2 protein levels in Sir3
162 overexpressing cells compared to WT (Fig EV2), indicating that Sir3 overexpression did not
163 impact Sae2 levels.

164 The dose dependent effect of Sir3 on NHEJ, and its suppression upon increasing
165 Sae2 expression, raises the possibility that Sir3 and Sae2 interact. Consistent with this
166 hypothesis, Sir3 overexpression drastically modified the nuclear distribution of Sae2-GFP.
167 Whereas Sae2-GFP exhibited a diffused nuclear signal in WT cells (Fig 2A), it accumulated
168 in a single bright focus upon Sir3 overexpression (Fig 2A). This bright focus resembled the
169 focus formed by telomeres, Rap1 and SIR proteins in response to Sir3 overexpression
170 (Ruault et al. 2011). Analysis of the localisation of Sae2-GFP and Sir3-mCherry confirmed
171 that the two proteins colocalize in a single cluster upon Sir3 overexpression (Fig 2A),
172 suggesting that they physically interact even in the absence of DSB.

173 Using a chromatin immunoprecipitation (ChIP) approach, we observed Sae2 bound to
174 chromosome ends in WT cells but not in cells lacking Sir3 (Fig 2B). Overexpression of Sir3
175 increased Sae2 interaction with telomeres and its spreading along subtelomeres suggesting
176 that Sir3 interacts with Sae2 on heterochromatin (Fig 2B).

177 Sae2-GFP pull-down of Sir3 was achieved in Sir3 overexpressing cells (Fig 2C), and
178 to a lesser extent in WT cells (Fig 2D). This further supports a physical interaction between
179 the two proteins. Furthermore, we observed Sae2-Sir3 interaction using a yeast two-hybrid
180 assay (Fig 3B, 3C and Appendix Fig S1), in agreement with a previous genome-wide screen
181 (Yu et al. 2008), and providing further evidence that the two proteins physically interact *in*

182 *vivo*. To characterize the domains involved in this interaction, we analysed the multiple
183 sequence alignments of both Sae2 and Sir3 proteins of the *Saccharomycetaceae* family and
184 delineated conserved subdomains (Fig 3A-C, EV3 and Appendix Fig S1). Yeast two-hybrid
185 assays screening of conserved subdomains revealed an interaction between the N-terminal
186 part of Sir3 AAA+ domain (Sir3^{SaID}; residues 531-723) and the Sae2 C-terminal domain
187 (Sae2^C, residues 173-345) (Fig 3A-C, EV3 and Appendix Fig S1). Sir3^{SaID} (for Sae2
188 Interaction Domain), overlaps with the previously defined Sir4 interacting domain (Fig 3A;
189 (King et al. 2006)). However, Sir4 was not required for the observed Sir3-Sae2 two-hybrid
190 interaction (Fig 3D).

191 To verify that the Sir3-Sae2 interaction was direct, we purified histidine-tagged Sae2^C
192 and GST-tagged Sir3^{SaID} fragments expressed in bacteria (Fig 3E) and performed *in vitro*
193 pull-down experiments. Sae2^C was retrieved with purified GST-Sir3^{SaID}, but not with GST
194 alone showing specific direct interaction (Fig 3F). Protein extracts used for this experiment
195 were supplemented with benzonase to remove DNA, showing that DNA did not mediate the
196 interaction and that direct protein interaction takes place between Sir3^{SaID} and Sae2^C.
197 Altogether, these results show that Sae2 directly interacts with Sir3. This interaction might be
198 the basis of the Sae2 inhibition observed upon Sir3 overexpression.

199 **Sae2 and Sir3 interaction prevents Sae2 functions and promotes NHEJ**

200 To functionally test whether Sae2-Sir3 interaction inhibits Sae2, we screened for Sir3
201 mutants without the capacity to interact with Sae2. To this end, we designed a two-hybrid
202 screen to select separation of function Sir3 mutants no longer interacting with Sae2, while
203 retaining interaction with Sir4. For this, we used a strain in which *HIS3* and *LacZ* reporter
204 genes associate with *GAL1* UAS and *lexAop* DNA targeting sequences respectively. This
205 allows for the simultaneous assessment of a positive interaction between two proteins,
206 alongside the loss of interaction between one of those proteins and a third (Fig 4A). We
207 transformed this strain with plasmids expressing *SIR4^C* fused to a *GAL4* binding domain and
208 *SAE2^C* fused to a *LexA* binding domain that bind upstream of *HIS3* and *LacZ* respectively. A
209 Sir4 binding partner fused to the Gal4 activating domain will thus activate the expression of
210 *HIS3*, whereas a Sae2 binding partner fused to the Gal4 activating domain will activate the
211 expression of *LacZ*.

212 We performed random mutagenesis of a Sir3 domain sufficient to interact with Sae2
213 and Sir4 (464-728 aa;(King et al. 2006)), and created a library of mutated *SIR3^{SaID}* fused to
214 the *GAL4* activating domain (GAD). This library was introduced into the screening strain and
215 Sir3 mutants still able to interact with Sir4 were selected based on their ability to grow on
216 media lacking histidine and supplemented with aminotriazole (-HIS + 3-AT). This step
217 eliminates non-sense or non-expressed GAD-SIR3^{SaID} mutants. X-Gal staining of His+

218 colonies allowed for the selection of white clones in which the GAD-SIR3^{SaiD} - LexABD-
219 Sae2^C interaction was lost.

220 Using this screen, we recovered a mutant deficient for Sir3-Sae2 interaction while proficient
221 for Sir3-Sir4 interaction. Sequencing of this mutant identified two point mutations T557I and
222 T598A followed by a frameshift at position 707 (*sir3*^{SaiD-1}; Fig 4B). These two residues are not
223 strictly conserved among the *Saccharomycetaceae* family, but T557 is flanked by a
224 conserved patch (Fig EV3). Subcloning of the individual mutations and secondary two-hybrid
225 tests showed that the mutation T557I alone is sufficient to impair the Sae2-Sir3 interaction
226 while preserving the Sir4-Sir3 interaction (*sir3*^{SaiD-T557I}; Fig 4C).

227 To test the functional consequences of Sir3-Sae2 interaction loss, we assessed
228 NHEJ in strains overexpressing either the WT or T557I mutant Sir3^{SaiD} fragment (Fig 5A).
229 High-level expression of the Sir3^{SaiD} fragment was sufficient to promote NHEJ and displayed
230 an epistatic relationship with the loss of Sae2 (Fig 5A and EV4). In contrast, high-level
231 expression of the mutated fragment had no effect, indicating that Sae2 inhibition by Sir3^{SaiD}
232 requires an intact Sae2-Sir3 interaction (Fig 5A).

233 **Strikingly, overexpression of the Sir3^{SaiD} fragment, which is sufficient to inhibit Sae2**
234 **(Fig 5A), did not promote Sae2 clustering (Fig 5B). This shows that Sae2 inhibition by Sir3 is**
235 **maintained, even when Sae2 is not trapped in the telomere cluster. These results indicate**
236 **that the inhibition of Sae2 is not only a secondary consequence of its sequestration by Sir3,**
237 **but rather suggests that Sir3-Sae2 interaction *per se* can inactivate Sae2.**

238 Insertion of the *T557I* mutation in the full-length *SIR3* gene reduced the ability of Sir3
239 to promote NHEJ when overexpressed (Fig 5C). This correlated with a loss of Sae2-sir3-
240 T557I colocalization (Fig 5D). Importantly, the point mutation does not affect the stability of
241 Sir3, and *sir3-T557I* overexpressing cells retained the ability to form the telomere
242 hypercluster (Fig 5D and EV4) and propagate subtelomeric heterochromatin (Fig 5E). In
243 contrast, Sae2-GFP no longer formed a single bright focus in *sir3-T557I* overexpressing cells
244 (Fig 5D), indicating that Sae2 clustering requires Sae2-Sir3 interaction. ***In vitro* the purified**
245 **Sir3^{SaiD} mutated fragment failed to interact with Sae2^C (Fig 5F). However,** the residual NHEJ
246 observed in cells overexpressing full length *sir3-T557I* suggests that it retains some
247 interaction with Sae2 *in vivo* (Fig 5C). This was confirmed by co-immunoprecipitation
248 experiments that showed a residual interaction with Sae2 *in vivo* (20 ± 10 % of the interaction
249 detected in WT, Fig 5F). Altogether, these data show that the Sir3^{SaiD} domain is sufficient to
250 interact with and inhibit Sae2, and that interaction between Sir3 and Sae2 is necessary and
251 sufficient to inhibit Sae2 activity.

252 **Sae2 and Sir4 compete for Sir3 binding**

253 To explore further the functional consequences of the Sir3-Sae2 interaction, we
254 assessed NHEJ in the absence of the SIR complex. Strains used lack the *HML* locus to
255 avoid indirect effects on NHEJ efficiency caused by pseudo-diploidization, as observed
256 following the derepression of the cryptic mating type loci in strains with *SIR* deletions (Aström
257 et al. 1999; Lee et al. 1999; Frank-Vaillant and Marcand 2001). Consistent with an inhibition
258 of Sae2 by Sir3 expressed at physiological levels, NHEJ was reproducibly decreased by ~2-
259 fold in *sir3Δ* mutants **both at chromosomal DSB sites and in plasmid rejoining assay** (Fig 6A
260 and 6B). In contrast, *sir4Δ* mutants exhibited a more than 2-fold increase in NHEJ relative to
261 WT, which was abolished by the additional loss of Sir3 (Fig 6A). This increase was epistatic
262 with *sae2Δ*, suggesting that Sae2 and Sir4 act in the same pathway to inhibit NHEJ.
263 Together, these results show that Sir3 is required to increase NHEJ in absence of Sir4 and
264 suggest that the regulation of Sae2 by Sir3 is involved. Consistently, the *sir3-T557I* mutant
265 impaired for interaction with and inhibition of Sae2, fails to increase NHEJ in absence of Sir4
266 (Fig 6A). Therefore, physiological levels of Sir3 are sufficient to inhibit Sae2, and Sir4 is able
267 to counteract this inhibition.

268 As Sae2 and Sir4 interact with the same Sir3 domain (Fig 3A), a competition between
269 Sir4 and Sae2 for Sir3 binding might explain NHEJ increase in cells lacking Sir4 and the
270 dependence of this increase on Sir3 and Sae2. If Sir4 and Sae2 compete for Sir3 binding,
271 overexpression of Sir4 should prevent Sir3-Sae2 interaction and counteract the increase in
272 NHEJ caused by Sir3 overexpression. We tested this hypothesis by Sir4 overexpression,
273 through genomic insertion of an additional copy of the *SIR4* gene under the control of a
274 strong promoter (*TEF1p*). As predicted, Sir4 overexpression alongside Sir3 overexpression
275 restored NHEJ to WT levels whereas it did not affect NHEJ in WT or *sae2Δ* cells (Fig 6C).
276 This indicates that Sir4 overexpression does not affect NHEJ by itself, but instead
277 counteracts Sir3-overexpression-mediated inhibition of Sae2. Expressing high levels of Sir4
278 was also sufficient to counteract the Sir3-overexpression induced clustering of Sae2 (Fig
279 6D), to disrupt the two-hybrid interaction detected between Sir3 and Sae2 (Fig 6E) and to
280 **decrease co-immunoprecipitation of Sir3 with Sae2 (Fig 6F)**, showing that Sir4 binding to
281 Sir3 counteracts Sir3-Sae2 interaction. Note that the favoured partner of Sir3 at
282 subtelomeres remains Sir4, since Sae2 overexpression had no effect on silencing (Fig EV5).
283 Collectively, this data is consistent with a model in which Sae2 is inactive when bound to
284 Sir3, but can be released by the competitive binding of Sir4 to Sir3.

285 **Sir3-mediated Sae2 inhibition mechanism**

286 How might Sir3-Sae2 interaction inhibit Sae2? Interestingly, the C-terminus of Sae2,
287 which we have demonstrated as sufficient for Sir3 interaction, also interacts with Rad50. This
288 interaction requires Sae2 C-terminus phosphorylation and is essential for stimulation of
289 Mre11 nuclease activity (Cannavo and Cejka 2014; Cannavo et al. 2018). Sir3 binding to
290 Sae2 could thus impair the interaction between Sae2 and MRX^{MRN} by steric hindrance, or by
291 impairing Sae2 C-terminus phosphorylation.

292 If Sir3 impairs Sae2-MRX^{MRN} interaction, Sae2 recruitment to DSB, which relies on its
293 interaction with MRX (Mojumdar et al. 2021), should be affected. Thus, we monitored Sae2
294 association with DSB by chromatin immunoprecipitation (ChIP) upon Sir3 overexpression.
295 We observed lower enrichment of Sae2 at DSB in Sir3 overexpressing cells compared to WT
296 (Fig 7A) while Sae2 binding to telomeres was not significantly affected (Fig 7B). These data
297 support the hypothesis that the trapping of Sae2 in the Sir3-mediated telomere cluster
298 impairs its ability to interact with MRX and to be recruited at DSB sites. In contrast,
299 overexpression of the Sir3^{Sald} domain which is sufficient to inhibit Sae2 (Fig 5A) did not
300 sequester Sir3 at telomeres (Fig 7B) and lead to a greater enrichment of Sae2 at DSB (Fig
301 7A). These results suggest that Sae2-MRX interaction is not affected by Sir3^{Sald}-Sae2
302 interaction *per se* when Sae2 is not trapped in the telomere cluster, and support the
303 hypothesis that Sir3-Sae2 interaction is sufficient to inhibit Sae2 activity. In agreement with
304 Sae2 inhibition by Sir3, independently of Sae2 binding to MRX at DSB, the absence of Sir3
305 does not significantly affect Sae2 enrichment at DSB (Fig 7A).

306 As stated above, Sir3 could inhibit Sae2 activity by preventing the phosphorylation of
307 the conserved CDK site at S267 of Sae2 C-terminus which is critical for its resection function
308 *in vitro* and *in vivo* (Huertas et al. 2008; Cannavo and Cejka 2014; Cannavo et al. 2018;
309 Zdravković et al. 2021). If this were the case, Sir3 inhibition should be relieved by the *sae2*-
310 *S267E* phosphomimic mutant. However, in contrast to this prediction, *sae2*-*S267E* interacts
311 with overexpressed Sir3 in the telomere cluster (Fig 7C) and is inhibited by Sir3
312 overexpression (Fig 7D). Altogether, these results indicate that Sir3 inhibits Sae2 once it has
313 been phosphorylated by CDK and is bound to MRX, and suggest that Sir3 affects the
314 subsequent step of *mre11* nuclease activation.

315 Discussion

316 Initiation of DSB end resection is a pivotal decision during DSB repair: it precludes the
317 “by default” repair by NHEJ and commits cells to repair by HR (Frank-Vaillant and Marcand
318 2002; Symington 2016). The effector of this irreversible pathway choice decision, the MRX-
319 Sae2 complex, is the focus of various regulatory inputs, including cell cycle phase (Huertas
320 et al. 2008; Huertas and Jackson 2009; Cannavo and Cejka 2014). Here we reveal an
321 unexpected role for Sir3 in impinging on this pathway choice. Sir3 physically interacts with

322 Sae2, inhibits its DSB-end resection initiation function and consequently increases MRX
323 retention at DSB sites and NHEJ efficiency.

324 Altogether, our results suggest that Sae2 inhibition relies on the inactivation of Sae2
325 following Sir3 binding to its C-terminus, the efficiency of which depends on the relative
326 abundance of each protein. **Sir3 binding per se does not inhibit Sae2 recruitment to DSB and
327 hence Sae2 interaction with MRX, but counteracts the ability of Sae2 to stimulate MRX
328 nuclease activity.** Sae2 has been shown to bind MRX^{MRN} through several independent
329 interactions involving Mre11, Xrs2 and Rad50 (Cannavo and Cejka 2014; Liang et al. 2015;
330 Cannavo et al. 2018). **Sir3 is unlikely to affect Sae2 interaction with Mre11, which fails to
331 interact with Sae2 C-terminal fragment in vitro (Cannavo et al. 2018), or with Xrs2, which
332 interacts with Sae2 N-terminus (Liang et al. 2015). It could however play on the binding of
333 Sae2 C-terminus to Rad50 heads, which is sufficient to stimulate Mre11 nuclease activity
334 (Cannavo et al. 2018). This hypothesis is further supported by the phenotype of the rad50S
335 mutant, which is reminiscent of the phenotype caused by Sir3-Sae2 interaction. Indeed, the
336 rad50S(K81I) mutation which affects Rad50-Sae2C interaction in vitro (Cannavo et al. 2018)
337 impairs Sae2-mediated MRX activation, but still allows strong recruitment of Sae2 to DSB in
338 vivo (Yu et al. 2018). Based on these observations, a hypothesis that awaits closer
339 examination is that Sir3 binding to Sae2 could impair the Sae2-Rad50 interaction required for
340 Sae2-mediated stimulation of Mre11 endonuclease activity.**

341 In addition, our data suggest that a pool of Sir3-bound Sae2 in subtelomeric
342 chromatin is prevented from activating MRX nuclease activity. One rationale behind limiting
343 the availability of Sae2 could be to limit resection, considering NHEJ is sufficient for the
344 repair of most DSB. Uncontrolled resection might also drive repair towards error-prone HR
345 (SSA, BIR) leading to loss of genetic information (Chen et al. 2013; Toledo et al. 2013; Lee
346 et al. 2016; Batté et al. 2017). Thus, tight control of the Sae2 pool that can engage in end
347 processing is needed to ensure genome integrity. The Sir3-bound pool of Sae2 at
348 subtelomeres is inactive, which limits resection and promotes NHEJ, ensuring genetic
349 integrity of subtelomeres. Sir3 impact at euchromatic DSB sites suggests that release of this
350 pool in response to DSB in regulating this pool could also have a more general role in DNA
351 repair. Consistently, the Sir3-bound pool of Sae2 at subtelomeres decreased in response to
352 DSB induction. Although release of Sae2 from telomeres might have been expected to
353 increase Sae2 DSB binding, the absence of Sir3 does not significantly improve Sae2
354 recruitment to DSB. This may not be surprising when considering that an excess of Sae2
355 increases MRX turnover at DSB (Yu et al. 2018) and may in turn limit Sae2
356 binding. Interestingly, our results echo previous studies showing that the SIR complex
357 dissociates from telomeres in S-G2 phase or upon damage induction (Martin et al. 1999;
358 Mills et al. 1999; McAinsh et al. 1999). Whether Sae2 and Sir3 are released from telomeres

359 as a complex remains to be determined experimentally. One possibility, considering that the
360 SIR complex in solution contains Sir2, Sir3 and Sir4 in a 1:1:1 molar ratio (Cubizolles et al.
361 2006), is that Sir3 once released from the telomeres is not able to accommodate Sae2
362 binding. Release of SIRs from telomeres could thus liberate a pool of Sae2 free to act at
363 DSB. A non exclusive scenario is that Sir3 which also associates with DSBs (Martin et al.
364 1999; Mills et al. 1999) controls Sae2 activity at DSB, limiting MRX activity to prevent
365 excessive resection. A timely regulation of Sae2-Sir3 interaction and of their release from
366 telomeres could participate in the fine regulation of active Sae2 at DSB.

367 Sae2-Sir3 interaction may also be relevant for telomere length regulation. During
368 telomere replication, Sae2 has a facultative role in facilitating the generation of the G rich 3'-
369 ssDNA, the telomerase substrate, and therefore in promoting telomere elongation (Bonetti et
370 al. 2009). Interestingly, in cells lacking Tel1, where telomerase recruitment depends
371 exclusively on Mec1 (Arnerić and Lingner 2007), and therefore possibly more so on
372 resection, Sae2 loss slightly shortens telomeres, compared to Sir3 loss, which elongates
373 them (Appendix Fig S2). In *tel1Δ* cells lacking Sae2, Sir3 loss does not impact telomere
374 length, suggesting that the telomere elongation observed in the presence of Sae2 might be a
375 consequence of increased Sae2 activity. Although the network of interactions at telomeres
376 does not allow us to rule out indirect effects, this data suggests that Sir3 could downregulate
377 Sae2 at telomeres.

378 The inhibition of Sae2 by Sir3 is suppressed by Sir4 overexpression suggesting that
379 Sir4 competes with Sae2 for Sir3 binding, and that this competition modulates the inhibition
380 of Sae2 by Sir3. This competition may explain how Sir4 loss increases NHEJ in euchromatin
381 (Fig 6A), simply by increasing the pool of Sae2 associated with and inhibited by Sir3. This
382 Sir4-dependent Sae2 activation could also promote telomere protection against NHEJ if
383 telomere-associated Sir3 molecules are in complex with Sir4.

384 The competition between Sae2 and Sir4 for Sir3 binding questions the relevance of
385 Sae2-Sir3 interaction in subtelomeric heterochromatin. Recent *in vitro* data support a
386 stoichiometry of two Sir3 molecules and one Sir2-4 dimer per nucleosome (Swygert et al.
387 2018). This suggests that one Sir3 molecule per nucleosome might not be interacting with
388 Sir4 on chromatin, leaving room for the binding and inhibition of Sae2 on heterochromatin-
389 bound Sir3. Consistently, we detect a Sir3-dependent Sae2 binding at subtelomeres in WT
390 cells (Fig 2B), and the inhibition of Sae2 activity at heterochromatic subtelomeric DSB (Fig
391 1A). The main function of Sir3-mediated Sae2 inhibition could thus be to protect
392 subtelomeres from resection, avoiding loss of genetic information and providing chromosome
393 end deprotection.

394 NHEJ is favoured at heterochromatic DSB, beyond Sae2 inhibition by Sir3, through a
395 mechanism that remains to be defined. The presence of the NHEJ factor KU at subtelomeres
396 (Martin et al. 1999), mediated by its interaction with Sir4 (Roy et al. 2004), could favour
397 NHEJ. Alternatively, the fact that heterochromatin limits resection, likely beyond MRX-Sae2
398 inhibition, may stabilise unprocessed DSB ends, therefore increasing NHEJ likelihood. It is
399 striking to note that NHEJ is favoured in heterochromatic subtelomeres, despite its strong
400 inhibition at telomere ends (Marcand et al. 2008). This dichotomy is conserved in mammalian
401 cells in which NHEJ is prevented at telomeres, but not near them (van Steensel et al. 1998;
402 Muraki et al. 2015). At yeast telomeres, a key NHEJ repressor is Sir4, which acts, at least in
403 part, in a Sir3 independent manner (Marcand et al. 2008; Roisé-Hamelin et al. 2021; Khayat
404 et al. 2021). Sir4 thus seems to have two opposite functions in NHEJ regulation depending
405 on chromosomal context: a strong repressive function at telomeres, and a stimulating
406 function at subtelomeres. Several hypotheses can be proposed to account for these
407 differences. Sir4 could be present in different amounts at subtelomeres and at telomeres.
408 Alternatively, Sir4 could adopt distinct conformations that would dictate its ability to inhibit
409 NHEJ depending on its binding partners at telomeres compared to subtelomeres.

410 In mammals, NHEJ is the prevalent repair mechanism in non-coding and silent
411 chromatin (Aymard et al. 2014), and in perinuclear heterochromatin (Lemaître et al. 2014).
412 Furthermore, CtIP interacts with BARD1, a HP1 binding partner, as well as CBX4, an E3
413 SUMO ligase subunit of the facultative heterochromatin Polycomb complex (Wu et al. 2015;
414 Soria-Bretones et al. 2017). Whether this is associated with regulation of CtIP activity
415 remains to be investigated. This data, together with our observations suggest that a
416 regulation of the MRX^{MRN}-Sae2^{CtIP} complex by the chromatin context might be a conserved
417 general principle.

418 Here, we provide the first insights into the mechanisms regulating DSB repair in yeast
419 heterochromatin. We show that the early resection step, which controls the choice between
420 NHEJ and HR, is tightly regulated in heterochromatin. Notably, there is a stringent regulation
421 of the MRX^{MRN} complexes potent end-resection activity, through the direct inhibition of
422 Sae2^{CtIP} by Sir3. Precise characterization of the Sir3-Sae2^{CtIP} binding interface will help in
423 understanding how Sae2 binds and activates MRX and may enable the design of specific
424 synthetic inhibitors towards Sae2^{CtIP}-mediated MRX^{MRN} activation, the cornerstone of
425 HR/NHEJ repair pathway choice.

426 **Methods**

427 **Plasmids**

428 Two-hybrid plasmids (*pACT2-SAE2*, *pACT2-SIR3^{SaID}*, *pACT2-SIR3*, *pACT2-SIR3⁴⁶⁴⁻⁷²⁸*,
429 *pGBT9-SIR3*, *pGBT9-SAE2^C*, *pGBT9-SIR3^{SaID}*, *pLexA-SAE2^C*) were constructed by inserting
430 the full length or appropriate fragments of *SAE2* and *SIR3* genes, amplified from W303
431 genomic DNA, in *pACT2*, *pGBT9* and *pBTM116* vectors digested by *Bam*HI by single strand
432 annealing cloning (SLIC, (Li and Elledge 2007)). To test interactions with Sir4, the *pGBD-C2-*
433 *SIR4* plasmid was used (Ehrentraut et al. 2011). *pACT2-sir3^{SaID-T5571}* and *pACT2-sir3-T5571*
434 were generated by rolling circle mutagenesis of *pACT2-SIR3^{SaID}* and *pACT2-SIR3* as
435 described in (Hansson et al. 2008). To overexpress Sae2, the *SAE2* gene was amplified from
436 W303 genomic DNA and inserted in *pRS423* digested by *Sall*-HF by SLIC (Li and Elledge
437 2007) to produce *pKD343*. To overexpress *SIR4* for NHEJ assays, *SIR4* amplified from
438 W303 genomic DNA was inserted by SLIC in *pKD431*, an integrative plasmid *pRS403* with a
439 *TEF1p* promoter, to generate *pKD432*. Genomic integration of the plasmids at *HIS3* is
440 possible after digestion by *Pst*I.

441 The *SIR3^{SaID(531-723)}* fragment was cloned under the T7 promoter into the vector *pNEAvG*
442 (Diebold et al. 2011) generating *pKD434* that allows GST- *Sir3^{SaID}* expression in bacteria.
443 *SAE2^C* was cloned into an adapted SUMO vector (*pKD435*) allowing His6-SUMO-Sae2^{Cter}
444 protein expression.

445 Mutagenesis of the sequence encoding Sir3⁴⁶⁴⁻⁷²⁸ using the GeneMorph II EZClone Domain
446 Mutagenesis Kit (Agilent, 200552-5) was performed by PCR on 9,5 µg of *pACT2-SIR3⁴⁶⁴⁻⁷²⁸*
447 with 20 cycles of amplification to allow low mutation rate. The PCR products were
448 subsequently subcloned by SLIC in *pACT2* and Sanger sequenced for mutation rate
449 estimation.

450 **Yeast strains**

451 All strains in this study are isogenic to W303 (*Mata* (or *Mata*α) *ADE2 leu2-3,112 his3-11,15*
452 *trp1-1 ura3-1*) and are listed in Appendix Table S1. For DSB induction the *I-SCEI* gene was
453 introduced in the yeast genome by transformation of the cells with *pKD144* (*pRS404-GAL1p-*
454 *I-SceI*) digested by *Pml*I to insert in *TRP1*. Gene deletions and insertions of strong
455 constitutive promoters (*GPDp*, *ADH1p*) were performed by PCR-based gene targeting
456 (Longtine et al. 1998).

457 The *mre11-H125N* allele was introduced in strains by crossing with the *LSY2854-21C* strain
458 (Chen et al. 2013). *Mre11-YFP* was introduced in strains by cross with the *W5089-6A* strain
459 (Kaiser et al. 2011). *Sae2-AAGRRIGDGAGLIN-GFP* was constructed by PCR gene targeting
460 on *pKT128* (Sheff and Thorn 2004). *SIR3-mCherry* was constructed by PCR gene targeting

461 on pSL1 (Léon et al. 2008) whose marker was replaced by Hygromycin B resistance (HPH^r),
462 with primers pr1328 and pr1329.

463 **Media and growth conditions**

464 Yeast strains were grown in rich medium (yeast extract–peptone–dextrose, YPD) or synthetic
465 complete (SC) medium lacking the appropriate amino acid at 30°C. Rich or synthetic medium
466 containing 2% lactate, 3% glycerol, 0.05% glucose (YPLGg) and lacking the appropriate
467 amino acids were used to grow the cells overnight prior the induction of I-SceI by plating onto
468 2% galactose plates or addition of 2% galactose to liquid culture.

469 **NHEJ efficiency measurement**

470 NHEJ efficiency measurement upon induction of a single DSB was performed as previously
471 described (Batté et al. 2017). Briefly, yeast strains were grown overnight in glycerol lactate
472 containing medium and plated on 2% galactose plates and on 2% glucose plates to
473 respectively induce or repress I-SceI. Survival on galactose was normalized with the cell
474 plating efficiency inferred from survival on glucose. Forty-eight isolated survivors from
475 galactose-containing plates were analysed by PCR and sequenced to characterize NHEJ
476 repair events. For each strain, at least three independent experiments were performed with
477 the corresponding controls.

478 For plasmid rejoining assays, 50 ng of a pRS316 vector restricted with Xho I was
479 transformed into cells by the lithium acetate transformation method in the presence of 50 µg
480 of denatured salmon sperm DNA as carrier DNA. The number of colonies formed after 3
481 days was normalized with the number of colonies obtained in a parallel transformation with a
482 circular pRS316 plasmid.

483 **Monitoring of DSB-flanking DNA and resection by real-time PCR**

484 Yeast cells were grown in 2 mL of YPD overnight. Cultures were then diluted in YPLGg and
485 grown to OD₆₀₀ = 0.3–0.8. The expression of I-SceI was induced by addition of galactose to
486 a final concentration of 2%. Cell samples were collected before and after induction at
487 different time points and DNAs were extracted. DNA measurements by quantitative PCRs
488 were performed using primers located 0.9 kb from the I-SceI cutting site or primers flanking
489 the I-SceI restriction site. A control primer pair was used to amplify a region of the *OGG1*
490 control locus. To correct for differences in DSB cleavage efficiency, the fraction of uncut DNA
491 (Fu) was subtracted from the fraction of total DNA at 1 kb (Ft) at each time point and
492 normalized to the fraction of cleaved DNA (Fc). Thus, cleaved remaining DNA at 1 kb = (Ft-
493 Fu)/Fc.

494 **Microscopy**

495 Live cell images were acquired using a wide-field inverted microscope (Leica DMI-6000B)
496 equipped with Adaptive Focus Control to eliminate Z drift, a 100x/1.4 NA immersion objective
497 with a Prior NanoScanZ Nanopositioning Piezo Z Stage System, a CMOS camera (ORCA-
498 Flash4.0; Hamamatsu) and a solid-state light source (SpectraX, Lumencore). The system is
499 piloted by MetaMorph software (Molecular Device).

500 For GFP-mCherry two-colour images, 19 focal steps of 0.20 μm were acquired sequentially
501 for GFP and mCherry with an exposure time of 100-200 ms using solid-state 475- and 575-
502 nm diodes and appropriate filters (GFP-mCherry filter; excitation: double BP, 450–490/550–
503 590 nm and dichroic double BP 500–550/600–665 nm; Chroma Technology Corp.).
504 Processing was achieved using ImageJ software (National Institutes of Health). YFP images
505 were acquired at indicated time points before and after DSB induction; 19 focal steps of
506 0.20 μm were acquired with an exposure time of 200 ms using a solid-state 500-nm diode
507 and a YFP filter (excitation 470–510 nm and dichroic 495 nm; Chroma Technology Corp.) All
508 the images shown are z projections of z-stack images.

509 **Two-hybrid analyses**

510 The yeast strain Y190 (Wade Harper et al. 1993) was transformed with 2 μ plasmids
511 encoding full length or truncated *SAE2* or *SIR3* fused to *GAL4* DNA binding (GBD) or
512 activation (GAD) domains, and selected on synthetic media without leucine and tryptophane.
513 Protein-protein interactions were assayed by growing the cells on selective media without
514 leucine, tryptophane and histidine, complemented with varying concentrations of 3-Amino-
515 1,2,4-triazole (3-AT), a competitive inhibitor of the *HIS3* gene. Blue coloration of the colony in
516 presence of X-Gal was used to assess protein interactions. The interactions were defined in
517 comparison to negative controls, carrying at least one empty vector. When the growth on
518 3AT containing medium was higher, or if the blue colour in presence of X-gal was stronger
519 than the negative control then an interaction between the two chimeric proteins was
520 assumed.

521 To screen for *SIR3* mutants a yeast strain (yKD1991) containing *LYS2::GAL1UAS-*
522 *HIS3TATA-HIS3* and *URA3::lexAop-lacZ* was constructed by crossing Y190 and CTY10-5d
523 (Bartel and Fields 1995). This strain was transformed with 2 μ plasmids encoding
524 mutagenized *SIR3*^{SalD} fused to *GAL4* DNA binding domain (GBD), *SAE2*^C fused *LexA* DNA
525 binding domain (LexABD) and *SIR4*^C to *GAL4* activation domain (GAD).

526 **Protein fragments cloning and purification**

527 The *Sir3*^{SalD} and *Sae2*^C peptides were expressed in *E. coli* strains BL21 (DE3) transformed
528 with pKD434 and pKD435 respectively. Expression of the peptides was induced by 0.5 mM
529 isopropyl- β -D-thiogalactoside (IPTG) for 3.5 h. Cells were harvested, suspended in lysis

530 buffer (50 mM Tris HCl pH8, 500 mM NaCl, 1 mM DTT, 10% glycerol, TritonX-100 x 1, 1
531 mg/mL lysozyme, 1 mM 4-(2-aminoethyl) benzenesulphonyl fluoride, 10 mM benzamide, 2
532 μ M pepstatin) and disrupted by sonication. Extract was cleared by centrifugation at 186000 x
533 g for 1 hour at 4°C.

534 *Sir3^{SaID}* containing extract was incubated at 4°C with GSH Sepharose resin (Cytiva,
535 Marlborough, MA) for 3h. Proteins were eluted with Buffer A (50 mM Tris HCl [pH8@4°C],
536 100 mM NaCl, 1 mM DTT) complemented with 30 mM glutathione. Fractions containing
537 GST-protein were pooled and applied to a 1 mL Resource Q column (Cytiva, Marlborough,
538 MA) equilibrated with buffer A. Protein was eluted with a 12 mL linear gradient of 0.05–1 M
539 NaCl. Purified GST-protein was stored at -80°C (see purification procedure scheme in
540 Appendix Fig S3).

541 *Sae2^C* extract was incubated with 2mL NiNTA resin (Qiagen, Germantown, MD) in batch,
542 rotated at 4°C for 2h and then poured into a Econo-Column® Chromatography column (Bio-
543 Rad, Hercules, CA). After extensive washing first with 80 mL of 20 mM Tris HCl [pH8@4°C],
544 500 mM NaCl, 0,5% NP40, 10% glycerol, 20 mM Imidazole followed by 80 mL of 20 mM Tris
545 HCl [pH8@4°C], 100 mM NaCl, 1 mM DTT, 10% glycerol, 20 mM Imidazole, on-column
546 cleavage was achieved by adding his-SUMO-Protease to a ratio of 80/1 (W/W). Untagged
547 *Sae2^{Cter}* was recovered from the flow through which was then applied to a 1 mL Resource S
548 column (Cytiva, Marlborough, MA) equilibrated with buffer B (20 mM Tris HCl [pH8@4°C], 50
549 mM NaCl, 1 mM DTT). Protein was eluted with a 20 mL linear gradient of 0.05–1 M NaCl.
550 Purified *Sae2^{Cter}* was stored at -80°C (see purification procedure scheme in Appendix Fig
551 S3).

552 **GST pull-down assays**

553 GST-*Sir3^{SaID}* fragment (10 μ g) or GST protein as a control (10 μ g) were immobilized on 20 μ L
554 Glutathione Sepharose 4B in 300 μ L of buffer A (50 mM Tris HCl [pH8@4°C], 150 mM NaCl,
555 1 mM DTT, 0.5 mM EDTA, 10% Glycerol), complemented with 2 mM MgCl₂ and 25 units of
556 benzonase for 90 minutes at 4°C. Beads were collected by centrifugation, and washed three
557 times with 300 μ L of buffer B (buffer A + 0.05% NP40). *Sae2^C* (10 μ g in 100 μ L buffer B
558 complemented with 2 mM MgCl₂ and 25 units of benzonase) was then added and incubated
559 for 150 minutes at 4°C with gentle agitation. The supernatant was removed and the beads
560 were washed two times with 300 μ L of buffer B. Proteins bound to the beads were then
561 eluted by addition of 20 μ L of 50 mM Tris-HCl [pH8@4°C], 150 mM NaCl, 1 mM DTT, 30 mM
562 glutathione. Proteins bound to the beads were resolved on 15% SDS-PAGE.

563 **Co-immunoprecipitation (Co-IP)**

564 Immunoprecipitations were performed as previously described (Forey et al. 2021) by lysing

565 40 to 50 OD600 units of exponential phase cultures. After sonication, clarification and
566 benzonase treatment (250 u/1 mg protein, SIGMA E1014-5KU) extracts were incubated 1h
567 at 4°C with 50 µL magnetic beads (Dynabeads M-280 sheep anti-mouse IgG ,invitrogen
568 11202D) coated with anti-GFP antibodies (Roche ref:11814460001). Proteins extracts were
569 resolved on 4-15% polyacrylamide gels, transferred on iBlot PVDF Membranes that were
570 probed with anti-GFP (1:1000, Roche ref:11814460001) and custom-made anti-Sir3
571 (1:10000;(Ruault et al. 2011)) antibodies.

572 **Chromatin immunoprecipitation (ChIP)**

573 Exponentially growing cells were crosslinked for 15 min with 1% formaldehyde (Sigma
574 F8775) at RT under agitation followed by quenching by addition of 0.125 M Glycine (Sigma
575 G8898) for 5 min under agitation. Cells were washed three times with cold 20mM Tris (4°C).
576 Dry pellets were frozen and conserved at -80°C. Cell pellets were resuspended in lysis buffer
577 (50 mM HEPES-KOH pH7.5, 140 mM NaCl, 5 mM EDTA, 1% Triton X-100, 0.1% Na-
578 deoxycholate) supplemented with 1 mM AEBSF (ThermoFisher 10563165) and anti-protease
579 (Complete ULTRA SIGMA ref: 5892988001) and lysed with a Precellys homogenizer. Whole
580 cell extracts were centrifuged 20 min at 13535 rpm and the chromatin containing pellet was
581 resuspended in 300 µL lysis buffer. Sonication of chromatin was performed using a
582 Diagenod Bioruptor at high setting for 3 cycles: 30 seconds ON + 30 seconds OFF.
583 Dynabeads (Panmous IgG, Invitrogen 11041) were washed three times and resuspended in
584 1 mL of PBS, 0.1% BSA and incubated with antibodies (10 µL anti-GFP (1:1000, Roche
585 ref:11814460001)/50 µL beads) on a rotating wheel for two hours at 4 C. Antibody-coupled
586 Dynabeads were washed three times with 1 mL of PBS, 0.1% BSA, and incubated with 400
587 µL of sonicated chromatin for 2h at 21°C. Beads were washed on ice with cold solutions: two
588 times with lysis buffer, once with wash buffer (10 mM Tris-HCl pH8, 0.25 M LiCl, 0.5% NP40,
589 5 mM EDTA, 0.5% Na-deoxycholate) and once with TE (10 mM Tris-HCl pH8, 1 mM EDTA).
590 Antibodies were un-coupled from beads with elution buffer (25 mM Tris-HCl pH8, 5 mM
591 EDTA, 0,5% SDS) for 20 min at 65 C. Eluates were collected and incubated overnight at
592 65°C for de-crosslinking. RNase A (Sigma, R65-13) and Pronase were added to samples
593 and incubated for 1 hour at 37 C. DNA was purified (DNA clean up kit, ThermoScientific
594 K0832) and eluted in 50 µl of elution buffer. The relative amount of DNA was quantified by
595 qPCR (primers listed in Appendix Table S2). Sae2-GFP enrichment was normalized to an
596 internal control locus (OGG1).

597 **Data availability**

598 This study includes no data deposited in external repositories.

599 **Acknowledgements**

600 We thank Z. Xu, A. Piazza, R. Koszul and Jamie Phipps for critical reading of this manuscript
601 and members of the Marcand and Dubrana laboratories for stimulating discussions. We
602 thank Susan Gasser, Ann E. Ehrenhofer-Murray, Lorraine Symington, Rodney Rothstein,
603 Laurent Maloisel and Florian Roisné-Hamelin for sharing plasmids and strains and Angela
604 Taddei for the custom-made rabbit polyclonal antibodies raised against full-length Sir3. This
605 work was supported by grants from Fondation pour la recherche médicale
606 (DEP20131128535), and from the European Research Council under the European
607 Community's Seventh Frame- work Program (FP7/2007 2013/European Research Council
608 Grant Agreement 281287), Fondation ARC pour la Recherche sur le Cancer (PJA-
609 20191209432), CEA Radiation biology program and EDF. HB was supported by a fellowship
610 from the CEA- IRTÉLIS PhD program.

611 **Author contributions**

612 HB, RC, CB, AB and KD performed experiments in yeast. DB, JD and XV performed the *in*
613 *vitro* experiments. SM designed and supervised the telomere length experiments and gave
614 critical input on NHEJ experiments. RG performed protein alignments that helped design
615 protein subdomains for yeast two hybrid and expression in bacteria. KD designed and
616 supervised the entire project with the help of HB. KD and HB wrote the manuscript with
617 critical input of the other authors.

618 **Conflict of interest**

619 The authors declare that they have no conflict of interest.

References:

- Allshire RC, Madhani HD (2018) Ten principles of heterochromatin formation and function. *Nat Rev Mol Cell Biol* 19:229–244. <https://doi.org/10.1038/nrm.2017.119>
- Arnerić M, Lingner J (2007) Tel1 kinase and subtelomere-bound Tbf1 mediate preferential elongation of short telomeres by telomerase in yeast. *EMBO Rep* 8:1080–1085. <https://doi.org/10.1038/sj.embor.7401082>
- Aström SU, Okamura SM, Rine J (1999) Yeast cell-type regulation of DNA repair. *Nature* 397:310. <https://doi.org/10.1038/16833>
- Aymard F, Bugler B, Schmidt CK, et al (2014) Transcriptionally active chromatin recruits homologous recombination at DNA double-strand breaks. *Nat Struct Mol Biol* 21:366–374. <https://doi.org/10.1038/nsmb.2796>
- Baroni E, Viscardi V, Cartagena-Lirola H, et al (2004) The Functions of Budding Yeast Sae2 in the DNA Damage Response Require Mec1- and Tel1-Dependent Phosphorylation. *Mol Cell Biol* 24:4151–4165. <https://doi.org/10.1128/MCB.24.10.4151-4165.2004>
- Bartel PL, Fields S (1995) Analyzing protein-protein interactions using two-hybrid system. *Methods Enzymol* 254:241–263. [https://doi.org/10.1016/0076-6879\(95\)54018-0](https://doi.org/10.1016/0076-6879(95)54018-0)
- Batté A, Brocas C, Bordelet H, et al (2017) Recombination at subtelomeres is regulated by physical distance, double-strand break resection and chromatin status. *EMBO J* 36:2609–2625. <https://doi.org/10.15252/embj.201796631>
- Bazzano D, Lomonaco S, Wilson TE (2021) Mapping yeast mitotic 5' resection at base resolution reveals the sequence and positional dependence of nucleases in vivo. *bioRxiv* 2021.02.27.433206. <https://doi.org/10.1101/2021.02.27.433206>
- Behrouzi R, Lu C, Currie MA, et al (2016) Heterochromatin assembly by interrupted Sir3 bridges across neighboring nucleosomes. *eLife* 5:. <https://doi.org/10.7554/eLife.17556>
- Bonetti D, Martina M, Clerici M, et al (2009) Multiple pathways regulate 3' overhang generation at *S. cerevisiae* telomeres. *Mol Cell* 35:70–81. <https://doi.org/10.1016/j.molcel.2009.05.015>
- Cannavo E, Cejka P (2014) Sae2 promotes dsDNA endonuclease activity within Mre11-Rad50-Xrs2 to resect DNA breaks. *Nature* 514:122–125. <https://doi.org/10.1038/nature13771>
- Cannavo E, Johnson D, Andres SN, et al (2018) Regulatory control of DNA end resection by Sae2 phosphorylation. *Nat Commun* 9:4016. <https://doi.org/10.1038/s41467-018-06417-5>
- Chen H, Lisby M, Symington LS (2013) RPA coordinates DNA end resection and prevents formation of DNA hairpins. *Mol Cell* 50:. <https://doi.org/10.1016/j.molcel.2013.04.032>

Chen H, Xue J, Churikov D, et al (2018) Structural Insights into Yeast Telomerase Recruitment to Telomeres. *Cell* 172:331-343.e13. <https://doi.org/10.1016/j.cell.2017.12.008>

Chen X, Tomkinson AE (2011) Yeast Nej1 Is a Key Participant in the Initial End Binding and Final Ligation Steps of Nonhomologous End Joining. *J Biol Chem* 286:4931–4940. <https://doi.org/10.1074/jbc.M110.195024>

Chiolo I, Minoda A, Colmenares SU, et al (2011) Double-strand breaks in heterochromatin move outside of a dynamic HP1a domain to complete recombinational repair. *Cell* 144:732–744. <https://doi.org/10.1016/j.cell.2011.02.012>

Clerici M, Mantiero D, Lucchini G, Longhese MP (2006) The *Saccharomyces cerevisiae* Sae2 protein negatively regulates DNA damage checkpoint signalling. *EMBO Rep* 7:212–218. <https://doi.org/10.1038/sj.embor.7400593>

Cubizolles F, Martino F, Perrod S, Gasser SM (2006) A homotrimer-heterotrimer switch in Sir2 structure differentiates rDNA and telomeric silencing. *Mol Cell* 21:825–836. <https://doi.org/10.1016/j.molcel.2006.02.006>

Dalby AB, Goodrich KJ, Pflingsten JS, Cech TR (2013) RNA recognition by the DNA end-binding Ku heterodimer. *RNA* 19:841–851. <https://doi.org/10.1261/rna.038703.113>

Diebold M-L, Fribourg S, Koch M, et al (2011) Deciphering correct strategies for multiprotein complex assembly by co-expression: application to complexes as large as the histone octamer. *J Struct Biol* 175:178–188. <https://doi.org/10.1016/j.jsb.2011.02.001>

Ehrentraut S, Hassler M, Oppikofer M, et al (2011) Structural basis for the role of the Sir3 AAA+ domain in silencing: interaction with Sir4 and unmethylated histone H3K79. *Genes Dev* 25:1835–1846. <https://doi.org/10.1101/gad.17175111>

Faure G, Jézéquel K, Roisé-Hamelin F, et al (2019) Discovery and Evolution of New Domains in Yeast Heterochromatin Factor Sir4 and Its Partner Esc1. *Genome Biol Evol* 11:572–585. <https://doi.org/10.1093/gbe/evz010>

Forey R, Barthe A, Tittel-Elmer M, et al (2021) A Role for the Mre11-Rad50-Xrs2 Complex in Gene Expression and Chromosome Organization. *Mol Cell* 81:183-197.e6. <https://doi.org/10.1016/j.molcel.2020.11.010>

Frank-Vaillant M, Marcand S (2001) NHEJ regulation by mating type is exercised through a novel protein, Lif2p, essential to the Ligase IV pathway. *Genes Dev* 15:3005–3012. <https://doi.org/10.1101/gad.206801>

Frank-Vaillant M, Marcand S (2002) Transient Stability of DNA Ends Allows Nonhomologous End Joining to Precede Homologous Recombination. *Mol Cell* 10:1189–1199. [https://doi.org/10.1016/S1097-2765\(02\)00705-0](https://doi.org/10.1016/S1097-2765(02)00705-0)

Fu Q, Chow J, Bernstein KA, et al (2014) Phosphorylation-Regulated Transitions in an Oligomeric State Control the Activity of the Sae2 DNA Repair Enzyme. *Mol Cell Biol* 34:778–793. <https://doi.org/10.1128/MCB.00963-13>

- Garcia V, Phelps SEL, Gray S, Neale MJ (2011) Bidirectional resection of DNA double-strand breaks by Mre11 and Exo1. *Nature* 479:241. <https://doi.org/10.1038/nature10515>
- Gartenberg MR, Smith JS (2016) The Nuts and Bolts of Transcriptionally Silent Chromatin in *Saccharomyces cerevisiae*. *Genetics* 203:1563–1599. <https://doi.org/10.1534/genetics.112.145243>
- Goodarzi AA, Noon AT, Deckbar D, et al (2008) ATM Signaling Facilitates Repair of DNA Double-Strand Breaks Associated with Heterochromatin. *Mol Cell* 31:167–177. <https://doi.org/10.1016/j.molcel.2008.05.017>
- Hansson MD, Rzeznicka K, Rosenbäck M, et al (2008) PCR-mediated deletion of plasmid DNA. *Anal Biochem* 375:373–375. <https://doi.org/10.1016/j.ab.2007.12.005>
- Hass EP, Zappulla DC (2015) The Ku subunit of telomerase binds Sir4 to recruit telomerase to lengthen telomeres in *S. cerevisiae*. In: *eLife*. <https://elifesciences.org/articles/07750>. Accessed 20 Apr 2021
- Hecht A, Strahl-Bolsinger S, Grunstein M (1996) Spreading of transcriptional repressor SIR3 from telomeric heterochromatin. *Nature* 383:92. <https://doi.org/10.1038/383092a0>
- Hoche A, Ruault M, Kaferle P, et al (2018) Expanding heterochromatin reveals discrete subtelomeric domains delimited by chromatin landscape transitions. *Genome Res* 28:1867–1881. <https://doi.org/10.1101/gr.236554.118>
- Huertas P, Cortés-Ledesma F, Sartori AA, et al (2008) CDK targets Sae2 to control DNA-end resection and homologous recombination. *Nature* 455:689–692. <https://doi.org/10.1038/nature07215>
- Huertas P, Jackson SP (2009) Human CtIP mediates cell cycle control of DNA end resection and double strand break repair. *J Biol Chem* 284:9558–9565. <https://doi.org/10.1074/jbc.M808906200>
- Kaiser GS, Germann SM, Westergaard T, Lisby M (2011) Phenylbutyrate inhibits homologous recombination induced by camptothecin and methyl methanesulfonate. *Mutat Res* 713:64–75. <https://doi.org/10.1016/j.mrfmmm.2011.05.016>
- Katan-Khaykovich Y, Struhl K (2005) Heterochromatin formation involves changes in histone modifications over multiple cell generations. *EMBO J* 24:2138–2149. <https://doi.org/10.1038/sj.emboj.7600692>
- Kegel A, Sjöstrand JOO, Åström SU (2001) Nej1p, a cell type-specific regulator of nonhomologous end joining in yeast. *Curr Biol* 11:1611–1617. [https://doi.org/10.1016/S0960-9822\(01\)00488-2](https://doi.org/10.1016/S0960-9822(01)00488-2)
- Khayat F, Cannavo E, Alshmary M, et al (2021) Inhibition of MRN activity by a telomere protein motif. *Nat Commun* 12:3856. <https://doi.org/10.1038/s41467-021-24047-2>

King DA, Hall BE, Iwamoto MA, et al (2006) Domain Structure and Protein Interactions of the Silent Information Regulator Sir3 Revealed by Screening a Nested Deletion Library of Protein Fragments. *J Biol Chem* 281:20107–20119. <https://doi.org/10.1074/jbc.M512588200>

Larson AG, Elnatan D, Keenen MM, et al (2017) Liquid droplet formation by HP1 α suggests a role for phase separation in heterochromatin. *Nature* 547:236–240. <https://doi.org/10.1038/nature22822>

Lee C-S, Wang RW, Chang H-H, et al (2016) Chromosome position determines the success of double-strand break repair. *Proc Natl Acad Sci U S A* 113:E146-154. <https://doi.org/10.1073/pnas.1523660113>

Lee K, Lee SE (2007) *Saccharomyces cerevisiae* Sae2- and Tel1-Dependent Single-Strand DNA Formation at DNA Break Promotes Microhomology-Mediated End Joining. *Genetics* 176:2003–2014. <https://doi.org/10.1534/genetics.107.076539>

Lee SE, Pâques F, Sylvan J, Haber JE (1999) Role of yeast SIR genes and mating type in directing DNA double-strand breaks to homologous and non-homologous repair paths. *Curr Biol CB* 9:767–770

Lemaître C, Grabarz A, Tsouroula K, et al (2014) Nuclear position dictates DNA repair pathway choice. *Genes Dev* 28:2450–2463. <https://doi.org/10.1101/gad.248369.114>

Léon S, Erpapazoglou Z, Haguenaer-Tsapis R (2008) Ear1p and Ssh4p Are New Adaptors of the Ubiquitin Ligase Rsp5p for Cargo Ubiquitylation and Sorting at Multivesicular Bodies. *Mol Biol Cell* 19:2379–2388. <https://doi.org/10.1091/mbc.E08-01-0068>

Li MZ, Elledge SJ (2007) Harnessing homologous recombination in vitro to generate recombinant DNA via SLIC. *Nat Methods* 4:251–256. <https://doi.org/10.1038/nmeth1010>

Liang J, Suhandynata RT, Zhou H (2015) Phosphorylation of Sae2 Mediates Forkhead-associated (FHA) Domain-specific Interaction and Regulates Its DNA Repair Function. *J Biol Chem* 290:10751–10763. <https://doi.org/10.1074/jbc.M114.625293>

Lisby M, Rothstein R (2004) Choreography of the DNA damage response: spatiotemporal relationships among checkpoint and repair proteins. *Cell* 118:699–713. <https://doi.org/10.1016/j.cell.2004.08.015>

Longtine MS, McKenzie A, Demarini DJ, et al (1998) Additional modules for versatile and economical PCR-based gene deletion and modification in *Saccharomyces cerevisiae*. *Yeast Chichester Engl* 14:953–961. [https://doi.org/10.1002/\(SICI\)1097-0061\(199807\)14:10<953::AID-YEA293>3.0.CO;2-U](https://doi.org/10.1002/(SICI)1097-0061(199807)14:10<953::AID-YEA293>3.0.CO;2-U)

Machida S, Takizawa Y, Ishimaru M, et al (2018) Structural Basis of Heterochromatin Formation by Human HP1. *Mol Cell* 69:385-397.e8. <https://doi.org/10.1016/j.molcel.2017.12.011>

- Mahaney BL, Lees-Miller SP, Cobb JA (2014) The C-terminus of Nej1 is critical for nuclear localization and non-homologous end-joining. *DNA Repair* 14:9–16. <https://doi.org/10.1016/j.dnarep.2013.12.002>
- Marcand S, Pardo B, Gratias A, et al (2008) Multiple pathways inhibit NHEJ at telomeres. *Genes Dev* 22:1153–1158. <https://doi.org/10.1101/gad.455108>
- Martin SG, Laroche T, Suka N, et al (1999) Relocalization of Telomeric Ku and SIR Proteins in Response to DNA Strand Breaks in Yeast. *Cell* 97:621–633. [https://doi.org/10.1016/S0092-8674\(00\)80773-4](https://doi.org/10.1016/S0092-8674(00)80773-4)
- Matsuzaki K, Shinohara A, Shinohara M (2008) Forkhead-Associated Domain of Yeast Xrs2, a Homolog of Human Nbs1, Promotes Nonhomologous End Joining Through Interaction With a Ligase IV Partner Protein, Lif1. *Genetics* 179:213–225. <https://doi.org/10.1534/genetics.107.079236>
- McAinsh AD, Scott-Drew S, Murray JA, Jackson SP (1999) DNA damage triggers disruption of telomeric silencing and Mec1p-dependent relocation of Sir3p. *Curr Biol CB* 9:963–966
- Meister P, Taddei A (2013) Building silent compartments at the nuclear periphery: a recurrent theme. *Curr Opin Genet Dev* 23:96–103. <https://doi.org/10.1016/j.gde.2012.12.001>
- Mills KD, Sinclair DA, Guarente L (1999) MEC1-Dependent Redistribution of the Sir3 Silencing Protein from Telomeres to DNA Double-Strand Breaks. *Cell* 97:609–620. [https://doi.org/10.1016/S0092-8674\(00\)80772-2](https://doi.org/10.1016/S0092-8674(00)80772-2)
- Mimitou EP, Symington LS (2008) Sae2, Exo1 and Sgs1 collaborate in DNA double-strand break processing. *Nature* 455:770–774. <https://doi.org/10.1038/nature07312>
- Mojumdar A, Adam N, Cobb JA (2021) Sgs1BLM independent role of Dna2DNA2 nuclease at DNA double strand break is inhibited by Nej1XLF
- Muraki K, Han L, Miller D, Murnane JP (2015) Processing by MRE11 is involved in the sensitivity of subtelomeric regions to DNA double-strand breaks. *Nucleic Acids Res* 43:7911–7930. <https://doi.org/10.1093/nar/gkv714>
- Palmbos PL, Daley JM, Wilson TE (2005) Mutations of the Yku80 C Terminus and Xrs2 FHA Domain Specifically Block Yeast Nonhomologous End Joining. *Mol Cell Biol* 25:10782–10790. <https://doi.org/10.1128/MCB.25.24.10782-10790.2005>
- Palmbos PL, Wu D, Daley JM, Wilson TE (2008) Recruitment of *Saccharomyces cerevisiae* Dnl4–Lif1 Complex to a Double-Strand Break Requires Interactions With Yku80 and the Xrs2 FHA Domain. *Genetics* 180:1809–1819. <https://doi.org/10.1534/genetics.108.095539>
- Renauld H, Aparicio OM, Zierath PD, et al (1993) Silent domains are assembled continuously from the telomere and are defined by promoter distance and strength, and by SIR3 dosage. *Genes Dev* 7:1133–1145. <https://doi.org/10.1101/gad.7.7a.1133>

Robert T, Vanoli F, Chiolo I, et al (2011) HDACs link the DNA damage response, processing of double-strand breaks and autophagy. *Nature* 471:74–79. <https://doi.org/10.1038/nature09803>

Roisé-Hamelin F, Pobiega S, Jézéquel K, et al (2021) Mechanism of MRX inhibition by Rif2 at telomeres. *Nat Commun* 12:2763. <https://doi.org/10.1038/s41467-021-23035-w>

Roy R, Meier B, McAinsh AD, et al (2004) Separation-of-function Mutants of Yeast Ku80 Reveal a Yku80p-Sir4p Interaction Involved in Telomeric Silencing. *J Biol Chem* 279:86–94. <https://doi.org/10.1074/jbc.M306841200>

Ruault M, De Meyer A, Loiodice I, Taddei A (2011) Clustering heterochromatin: Sir3 promotes telomere clustering independently of silencing in yeast. *J Cell Biol* 192:417–431. <https://doi.org/10.1083/jcb.201008007>

Ruault M, Scolari VF, Lazar-Stefanita L, et al (2021) Sir3 mediates long-range chromosome interactions in budding yeast. *Genome Res* 31:411–425. <https://doi.org/10.1101/gr.267872.120>

Sheff MA, Thorn KS (2004) Optimized cassettes for fluorescent protein tagging in *Saccharomyces cerevisiae*. *Yeast Chichester Engl* 21:661–670. <https://doi.org/10.1002/yea.1130>

Soria-Bretones I, Cepeda-García C, Checa-Rodríguez C, et al (2017) DNA end resection requires constitutive sumoylation of CtIP by CBX4. *Nat Commun* 8:113. <https://doi.org/10.1038/s41467-017-00183-6>

Strahl-Bolsinger S, Hecht A, Luo K, Grunstein M (1997) SIR2 and SIR4 interactions differ in core and extended telomeric heterochromatin in yeast. *Genes Dev* 11:83–93. <https://doi.org/10.1101/gad.11.1.83>

Strom AR, Emelyanov AV, Mir M, et al (2017) Phase separation drives heterochromatin domain formation. *Nature* 547:241–245. <https://doi.org/10.1038/nature22989>

Swygert SG, Senapati S, Bolukbasi MF, et al (2018) SIR proteins create compact heterochromatin fibers. *Proc Natl Acad Sci* 115:12447–12452. <https://doi.org/10.1073/pnas.1810647115>

Symington LS (2016) Mechanism and regulation of DNA end resection in eukaryotes. *Crit Rev Biochem Mol Biol* 51:195–212. <https://doi.org/10.3109/10409238.2016.1172552>

Toledo LI, Altmeyer M, Rask M-B, et al (2013) ATR Prohibits Replication Catastrophe by Preventing Global Exhaustion of RPA. *Cell* 155:1088–1103. <https://doi.org/10.1016/j.cell.2013.10.043>

Tsabar M, Eapen VV, Mason JM, et al (2015) Caffeine impairs resection during DNA break repair by reducing the levels of nucleases Sae2 and Dna2. *Nucleic Acids Res* 43:6889–6901. <https://doi.org/10.1093/nar/gkv520>

Tsouroula K, Furst A, Rogier M, et al (2016) Temporal and Spatial Uncoupling of DNA Double Strand Break Repair Pathways within Mammalian Heterochromatin. *Mol Cell* 63:293–305. <https://doi.org/10.1016/j.molcel.2016.06.002>

Valencia M, Bentele M, Vaze MB, et al (2001) NEJ1 controls non-homologous end joining in *Saccharomyces cerevisiae*. *Nature* 414:666–669. <https://doi.org/10.1038/414666a>

van Steensel B, Smogorzewska A, de Lange T (1998) TRF2 protects human telomeres from end-to-end fusions. *Cell* 92:401–413

Wade Harper J, Adami GR, Wei N, et al (1993) The p21 Cdk-interacting protein Cip1 is a potent inhibitor of G1 cyclin-dependent kinases. *Cell* 75:805–816. [https://doi.org/10.1016/0092-8674\(93\)90499-G](https://doi.org/10.1016/0092-8674(93)90499-G)

Wu W, Nishikawa H, Fukuda T, et al (2015) Interaction of BARD1 and HP1 is required for BRCA1 retention at sites of DNA damage. *Cancer Res* 75:1311–1321. <https://doi.org/10.1158/0008-5472.CAN-14-2796>

Yu H, Braun P, Yildirim MA, et al (2008) High-quality binary protein interaction map of the yeast interactome network. *Science* 322:104–110. <https://doi.org/10.1126/science.1158684>

Yu T-Y, Kimble MT, Symington LS (2018) Sae2 antagonizes Rad9 accumulation at DNA double-strand breaks to attenuate checkpoint signaling and facilitate end resection. *Proc Natl Acad Sci U S A* 115:E11961–E11969. <https://doi.org/10.1073/pnas.1816539115>

Zdravković A, Daley JM, Dutta A, et al (2021) A conserved Ctp1/CtIP C-terminal peptide stimulates Mre11 endonuclease activity. *Proc Natl Acad Sci U S A* 118:. <https://doi.org/10.1073/pnas.2016287118>

Figure Legends

Figure 1 : Sir3 overexpression inhibits Sae2 and increases error-prone NHEJ

A. Schematic representation of the assay used to estimate error-prone NHEJ at euchromatic DSB.

B. Survival frequencies observed after DSB induction at TEL6R in WT, *dnI4Δ*, *sir4Δ* cells, expressing or not high levels of Sir3p (*oeSir3* and WT respectively). Error bars indicate survival standard error (SEM) of at least three independent experiments.

C. Survival frequencies observed after DSB induction at LYS2 in the indicated strains. Error bars indicate survival standard error (SEM) of at least three independent experiments.

D. Schematic representation of the LYS2 locus with primers located at 1 kb from the I-SceI site for the DNA measurements (blue arrows).

E. DNA levels measured at 0.2 kb from the I-SceI cut site at LYS2 after 2h DSB induction by qPCR in WT and *sae2Δ* cells expressing or not high levels of Sir3p (*oeSir3* and WT

respectively). DNA levels were normalized to DNA levels at the OGG1 locus and corrected for differences in DSB cleavage efficiency (see Materials and Methods for details). Error bars represent the standard deviation (SD) of three independent experiments.

F. Representative images of Mre11-YFP foci in response to an I-SceI-induced DSB at LYS2 in WT cells, expressing or not high levels of Sir3p (oeSir3 and WT respectively). Scale bars are 2 μ m.

G. Quantification of cells with DSB induced Mre11-YFP foci after DSB induction at LYS2 I-SceI cleavage site in WT, sae2 Δ and Sir3 overexpressing (oeSir3) strains. Error bars indicate survival standard error (SEM) of at least three independent experiments.

H. Survival frequencies after DSB induction at LYS2 locus, in strains where SIR3 is expressed from its native, pADH1 or pGPD promoters respectively and in which SAE2 is expressed or not from a high copy number 2 μ plasmid. Fold increase in Sir3 protein by pAHD1 or pGPD (Hoche et al 2018) is indicated. Error bars indicate survival standard error (SEM) of at least three independent experiments.

Data information: Significance was determined using 2-tailed, unpaired Student's t test. *P-value 0.01 to 0.05, significant; **P-value 0.001 to 0.01, very significant; ***P-value 0.0001 to 0.001, extremely significant; ****P < 0.0001, extremely significant; P \geq 0.05, not significant (ns).

Figure 2: Sir3 and Sae2 physically interact

A. Representative images of Sir3-mCherry and Sae2-GFP signal in WT and SIR3 overexpressing cells. Scale bars are 2 μ m.

B. Sir3-binding at TEL6R in untagged, WT, sir3 Δ cells or in cells overexpressing Sir3 (oeSir3). Binding is probed by ChIP-qPCR 0.2 (red arrows) and 1kb (blue arrows) from telomeres and at the OGG1 control locus using antibodies against Sae2-GFP. The mean of three independent biological replicates is shown and error bars correspond to the variation between replicates.

C. Co-immunoprecipitation between Sir3 and Sae2-GFP from cells overexpressing Sir3, analysed by Western blot with anti-GFP and anti-Sir3 antibodies.

D. Co-immunoprecipitation between Sir3 and Sae2-GFP from WT cells using antibodies against Sae2-GFP, analysed by Western blot.

Figure 3: Direct physical interaction between Sir3^{SaID} and Sae2^C domains

A. Schematic representation of Sir3 and Sae2 protein domains.

B. Delineation of the Sir3 domain responsible for interaction with Sae2 by two-hybrid assays. The GAL4-BD fusions with indicated Sir3 fragments were tested in combination with a GAL4-AD-Sae2 fusion; "+" indicates an interaction.

- C. Delineation of the Sae2 domain responsible for interaction with Sir3 by two-hybrid assays. The GAL4-BD fusions with indicated Sae2 fragments were tested in combination with a GAL4-AD-Sir3 fusion; “+” indicates an interaction.
- D. Yeast two-hybrid interaction analysis between Sae2^C and Sir3^{SalD} domains in WT or sir4Δ cells. Growth on -His + 3AT and blue coloration on X-gal indicate an interaction.
- E. Comassie-stained gel of purified GST-Sir3^{SalD} and Sae2^C peptides.
- F. Representative silver-stained gels of in vitro GST-pulldown of GST or GST-Sir3^{SalD} and Sae2^C purified peptides. Control: Sae2^C (300 ng, lane 4).

Figure 4: The T557I point mutation in Sir3 abolishes Sae2-Sir3 interaction

- A. Schematic representation of the assay used to screen for SIR3 mutants deficient for Sae2 interaction while maintaining interaction with Sir4. The SIR3^{SalD} fragment (464-728) was mutagenized by PCR, cloned in the pACT2 two hybrid plasmid and transformed into the reporter strain along with plasmids expressing LexA-BD-SAE2^C and GAL4-BD-SIR4^C fusion proteins. The reporter strain (yKD1991) bears a Gal4 binding sequence (Gal4BD) upstream of a HIS3 reporter gene, and a LexA binding sequence (LexABD) precedes a LacZ reporter gene. Transformants in which the gal4-BD-Sir4^C and Sir3^{SalD}-gal4-AD fragments interact were selected for HIS3 expression on -HIS + 3AT medium and subsequently screened for LacZ expression upon X-gal coloration. Cells showing no LacZ expression were collected and the mutated sir3^{SalD}-GAL4-AD was retrieved and sequenced.
- B. Representative images of two hybrid assays in the yKD1991 strain testing the interaction of the WT or the mutant SIR3^{SalD} fragment isolated from the screen with SAE2^C or SIR4^C.
- C. Representative images of two hybrid assays testing the interaction of the WT or the mutant SIR3^{SalDT557I} fragment with SAE2^C or SIR4^C.

Figure 5: Sir3-Sae2 interaction prevents Sae2 function and promotes NHEJ

- A. Survival frequencies after DSB induction at LYS2 locus in WT or sae2Δ strains where the Sir3^{SalD} or Sir3^{SalDT557I} domains are overexpressed from a GPD promoter at the SIR3 locus. Error bars indicate survival standard error (SEM) of at least three independent experiments.
- B. Representative images of Sae2-GFP in WT cells and in cells overexpressing either full-length Sir3 or the sir3SalD domain. Scale bars are 2 μm.
- C. Survival frequencies after DSB induction at LYS2 locus in the indicated strains. Error bars indicate survival standard error (SEM) of at least three independent experiments.
- D. Representative images of Sir3-mCherry and Sae2-GFP signal in cells overexpressing Sir3 and sir3T557I. Scale bars are 2 μm.

E. Telomeric silencing assay at TEL7L in WT, sir4 Δ , sir3T557I cells, cells overexpressing SIR3 (oeSIR3) or sir3T557I (oesir3T557I). Growth on 5-FOA plates reflects telomeric silencing.

F. Representative silver-stained gels of in vitro GST-pulldown of GST or GST-Sir3^{SaID}, GST-sir3-T557I^{SaID} and Sae2^C purified peptides. Control: Sae2^C (300 ng, lane 6).

G. Co-immunoprecipitation between Sae2-GFP and Sir3 from untagged, Sae2-GFP WT cells, and Sae2-GFP cells overexpressing WT Sir3 (oeSir3, WT), Sae2-GFP sir3 Δ or Sae2-GFP overexpressing the sir3-T557I mutant (oeSir3, T557I) using antibodies against Sae2-GFP, analysed by Western blot with anti-GFP and anti-Sir3 antibodies.

Data information: Significance was determined using 2-tailed, unpaired Student's t test. *P-value 0.01 to 0.05, significant; **P-value 0.001 to 0.01, very significant; ***P-value 0.0001 to 0.001, extremely significant; ****P < 0.0001, extremely significant; P \geq 0.05, not significant (ns).

Figure 6: Sir3-Sae2 interaction is modulated by Sir4.

A. Survival frequencies after DSB induction at LYS2 locus in the indicated strains. Error bars indicate survival standard error (SEM) of at least three independent experiments.

B. Plasmid cleaved by Xho I was transformed into strains and NHEJ efficiency was measured. Error bars indicate survival standard error (SEM) of at least three independent experiments.

C. Survival frequencies after DSB induction at LYS2 locus in the indicated strains. Insertion of the strong TEF1p promoter upstream of the SIR4 ORF leads to Sir4 overexpression. Insertion of the ADH1p promoter upstream of SIR3 leads to mild Sir3 overexpression. Error bars indicate survival standard error (SEM) of at least three independent experiments.

D. Representative images of Sae2-GFP in cells overexpressing Sir3 (oeSir3) and expressing or not high levels of Sir4 (oeSir4). Scale bars are 2 μ m.

E. Representative images of two hybrid assays testing the interaction between the full-length Sir3 and full-length Sae2 proteins in WT cells expressing or not high levels of Sir4 (oeSir4 and WT respectively).

F. Co-immunoprecipitation between Sae2-GFP and Sir3 from untagged, Sae2-GFP cells overexpressing Sir3 and expressing or not high levels of Sir4 (oeSir4).

Data information: Significance was determined using 2-tailed, unpaired Student's t test. *P-value 0.01 to 0.05, significant; **P-value 0.001 to 0.01, very significant; ***P-value 0.0001 to 0.001, extremely significant; ****P < 0.0001, extremely significant; P \geq 0.05, not significant (ns).

Figure 7: Modulation of Sae2 recruitment and activity by Sir3

A. Relative fold enrichment of Sae2 at 0.2 kb from I-SceI site was evaluated by qPCR after ChIP with anti-GFP antibodies. The error bars indicate the variation between at least three biological replicas.

B. Relative fold enrichment of Sae2 at 0.2 kb from *TEL6R* after DSB induction at the *LYS2* I-SceI site was evaluated by qPCR after ChIP with anti-GFP antibodies. The error bars indicate the variation between at least three biological replicas.

C. Representative images of *sae2-E267E* mutant cells overexpressing or not full-length Sir3. Scale bars are 2 μ m.

D. Survival frequencies after DSB induction at *LYS2* locus in *sae2-E267E* mutant cells overexpressing or not full-length Sir3 (oeSir3).

Data information: Significance was determined using 2-tailed, unpaired Student's t test. *P-value 0.01 to 0.05, significant; **P-value 0.001 to 0.01, very significant; ***P-value 0.0001 to 0.001, extremely significant; ****P < 0.0001, extremely significant; P \geq 0.05, not significant (ns).

Expanded View Figure Legends

Figure EV1:

A. Survival frequencies and characterisation of the repair events after induction of a DSB at *LYS2* in absence of recombination substrate.

B. Survival frequencies and characterisation of the repair events after induction of a DSB at *TEL6R* in absence of recombination substrate.

NHEJ stands for error-prone end joining events detected by a PCR product that cannot be cleaved *in vitro* by I-SceI. No DSB corresponds to survivors giving a PCR product that can be cleaved by I-SceI *in vitro* showing that they failed to induce I-SceI. Other gathers survivors in which no PCR product was obtained suggesting that repair occurred through other mechanisms. PCR products corresponding to NHEJ events were sequenced and exhibit patterns typical of NHEJ repair (rejoining with 1 to 9 bp deletion between sequences showing no or limited homology).

C. DNA levels measured at 1 kb from the I-SceI cut site at *LYS2* after 2h DSB induction by qPCR in WT and *sae2* Δ cells expressing or not high levels of Sir3p (oeSir3 and WT respectively). DNA levels were normalized to DNA levels at the *OGG1* locus and corrected for differences in DSB cleavage efficiency (see Materials and Methods for details). Error bars represent the standard deviation (SD) of three independent experiments.

Figure EV2:

Western blot analysis with anti-GFP antibodies of whole cell protein extracts prepared from stationary phase cells. The 80kDa band detected by mab414 is used as a loading control.

Figure EV3:

A. Multiple sequence alignment of the Sir3^{sap} domain of the *Saccharomycetaceae* family. NCBI RefSeq identifiers are given in parentheses. Below, ribbon representation of the Xray structure of the Sir3^{sap} domain (rainbow colors) and a surface projection of the conservation as calculated by the rate4site algorithm (Pupko et al, 2002) with a white-yellow-red color gradient highlighting the most conserved region in red.

B. Multiple sequence alignment of the Sae2^c domain of the *Saccharomycetaceae* family. NCBI RefSeq identifiers are given in parentheses.

Figure EV4:

A, B. Western blot analysis with Sir3 antibodies of protein extracts prepared from stationary phase cells of the indicated strains.

Dps1 is used as a loading control. *Asterisk marks cross reacting Orc1 detected by the Sir3 antibody.

Figure EV5:

A. Telomeric silencing assay at TEL7L in WT and sir4 Δ cells overexpressing SAE2 (2 μ -Sae2) or not (2 μ). Increased growth on 5-FOA or decreased growth on -URA plates reflects an increase in telomeric silencing.

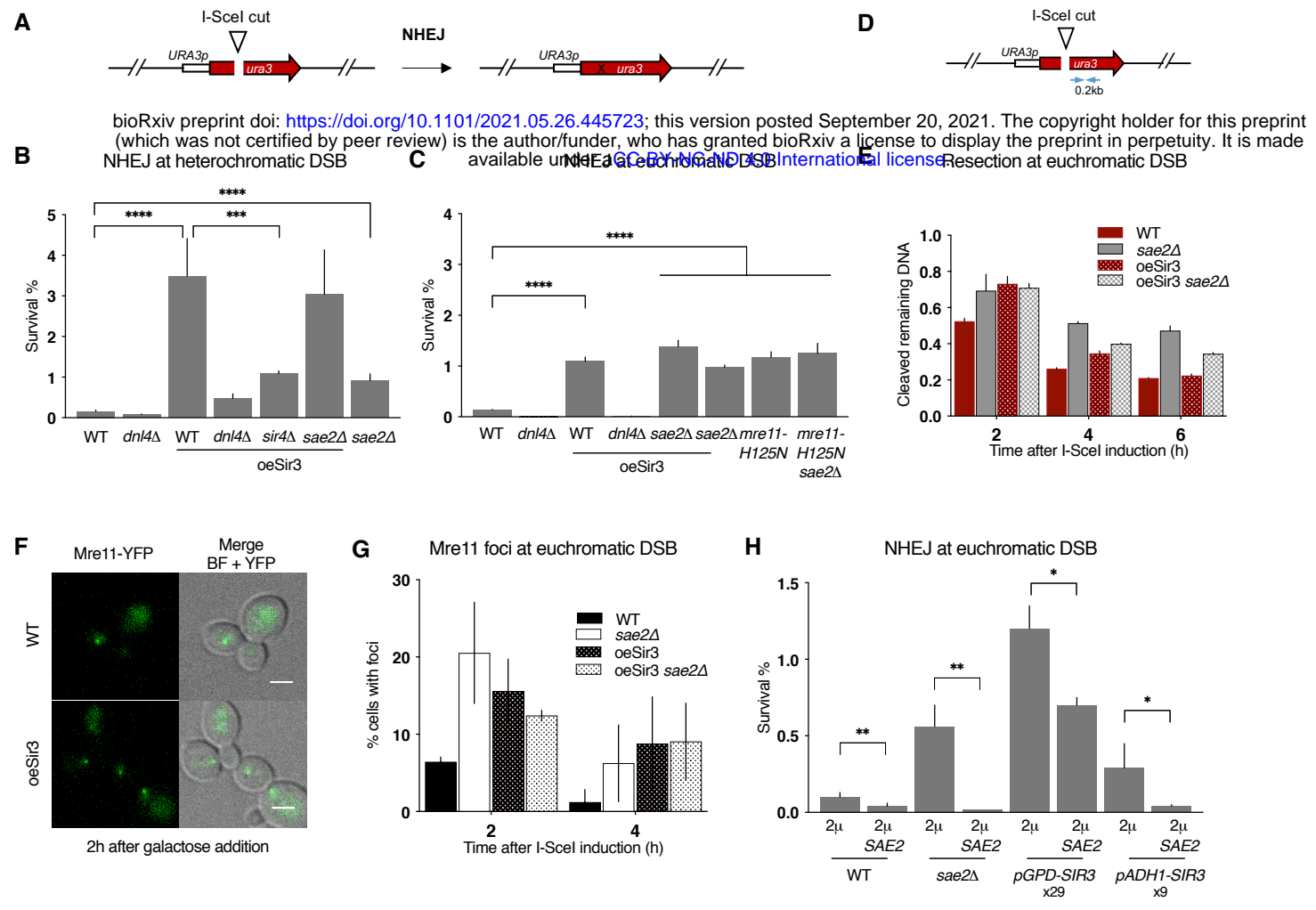


Figure 1

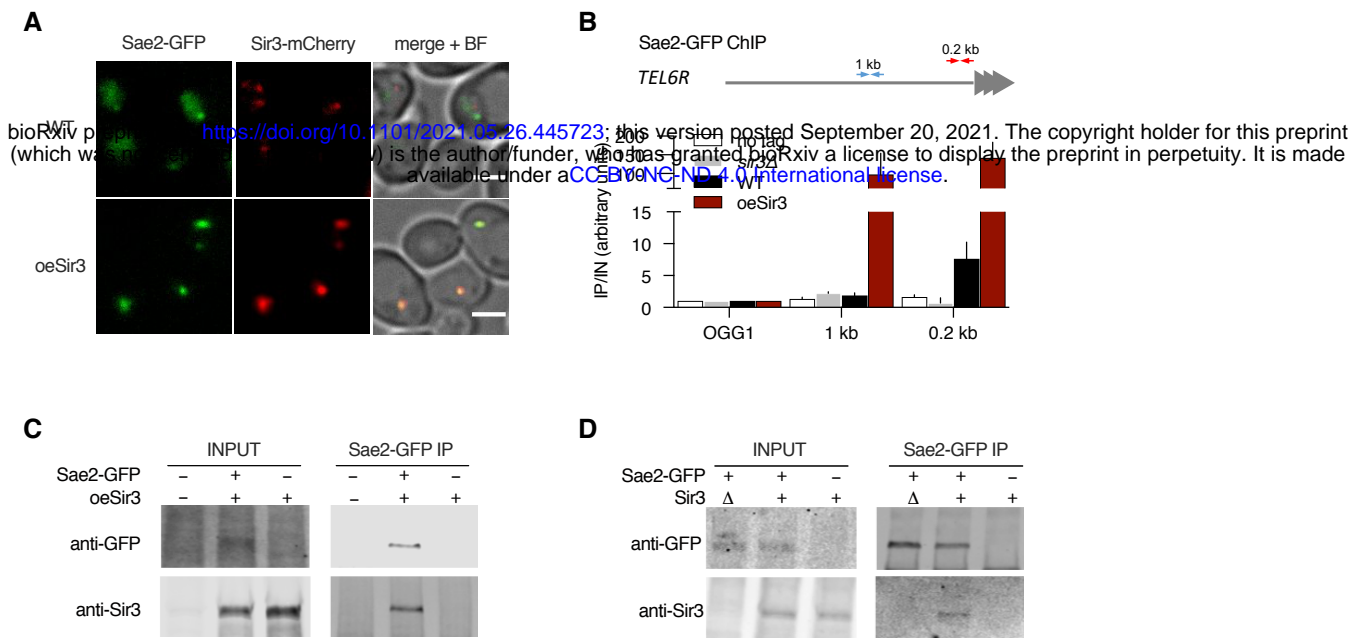
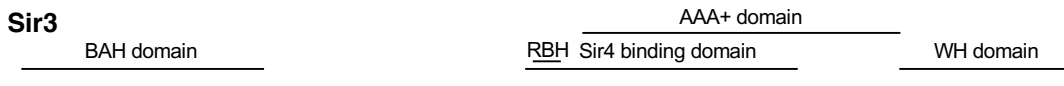
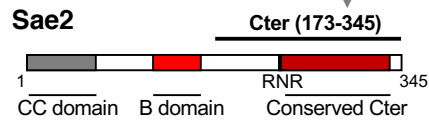
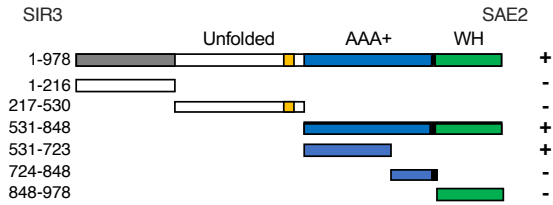
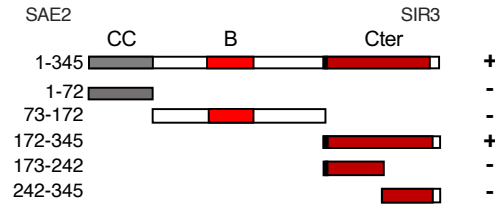
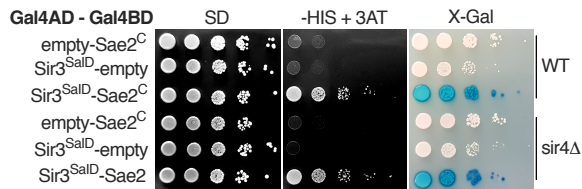
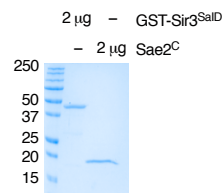
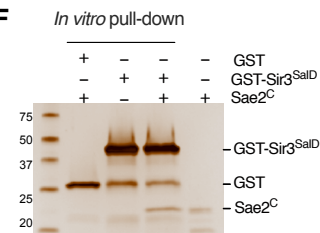


Figure 2

A**Sir3**

bioRxiv preprint doi: <https://doi.org/10.1101/2021.05.26.445723>; this version posted September 20, 2021. The copyright holder for this preprint (which was not certified by peer review) is the author/funder, who has granted bioRxiv a license to display the preprint in perpetuity. It is made available under a [CC-BY-NC-ND 4.0 International license](https://creativecommons.org/licenses/by-nc-nd/4.0/).

**B** Two-hybrid**C** Two-hybrid**D****E****F**

A

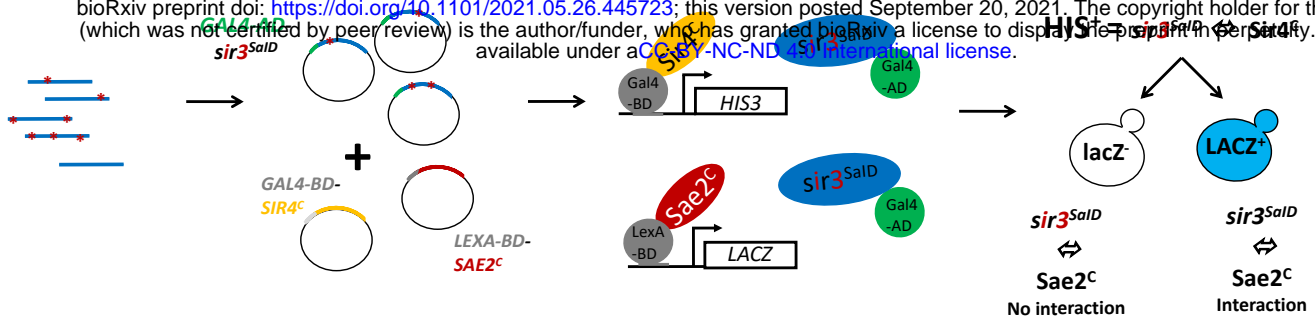
**1 - SIR3⁴⁶⁴⁻⁷²⁸ PCR
MUTAGENESIS**

2 - CLONING

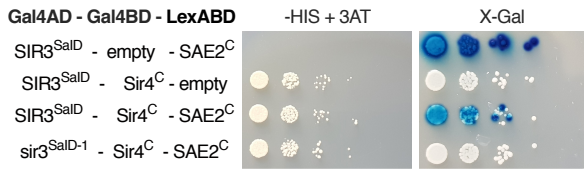
**3 - TRANSFORMATION IN
S. CEREVISIAE Y2H STRAIN**

**4 - SELECTION OF HIS+
COLONIES AND X-GAL
SCREENING**

bioRxiv preprint doi: <https://doi.org/10.1101/2021.05.26.445723>; this version posted September 20, 2021. The copyright holder for this preprint (which was not certified by peer review) is the author/funder, who has granted bioRxiv a license to display the preprint in perpetuity. It is made available under aCC-BY-NC-ND 4.0 International license.



B



C

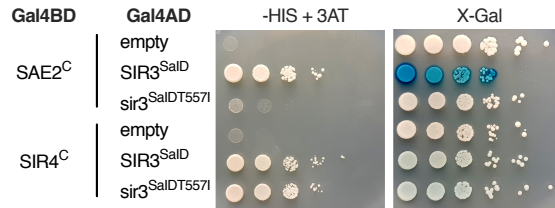


Figure 4

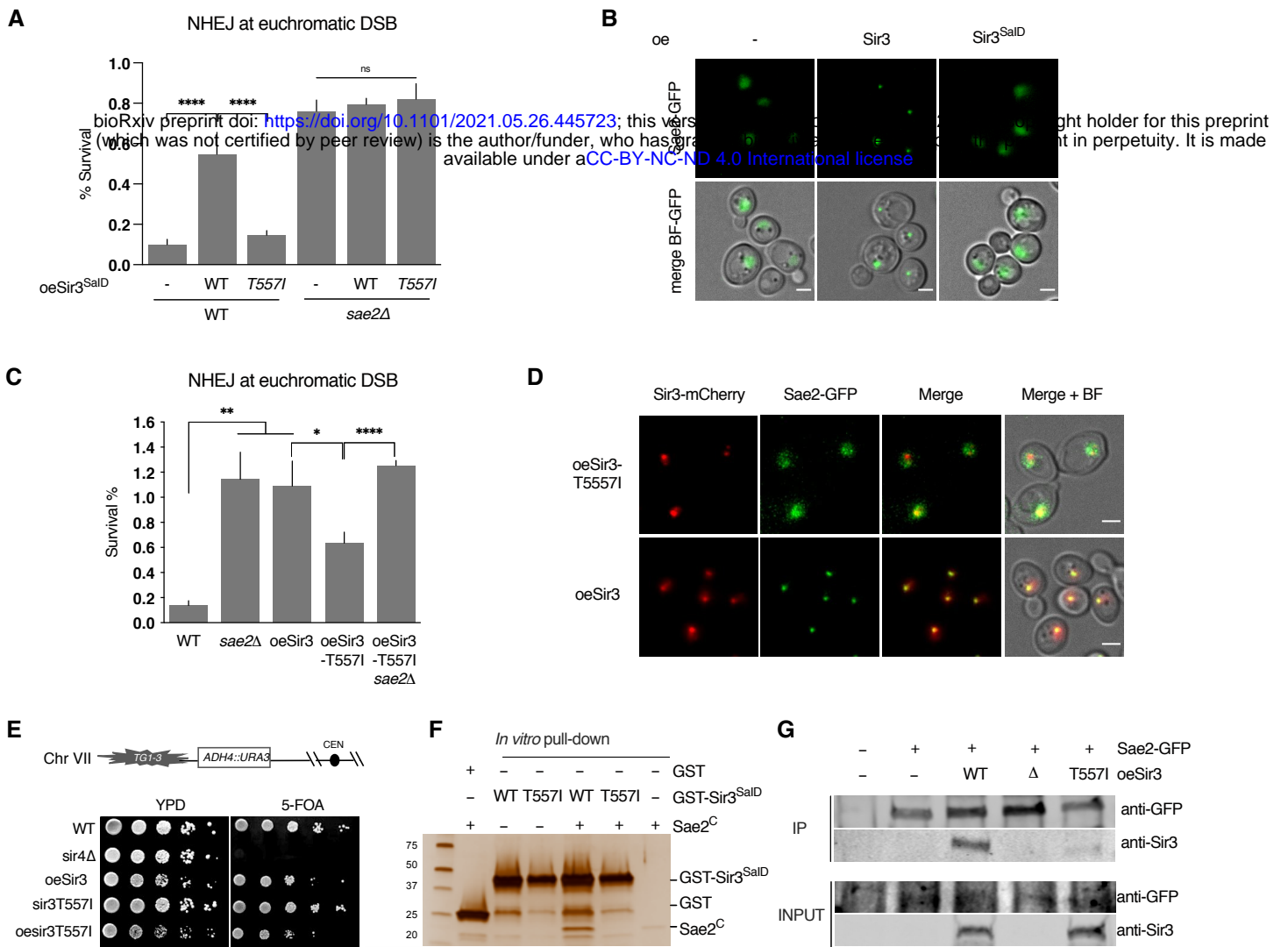


Figure 5

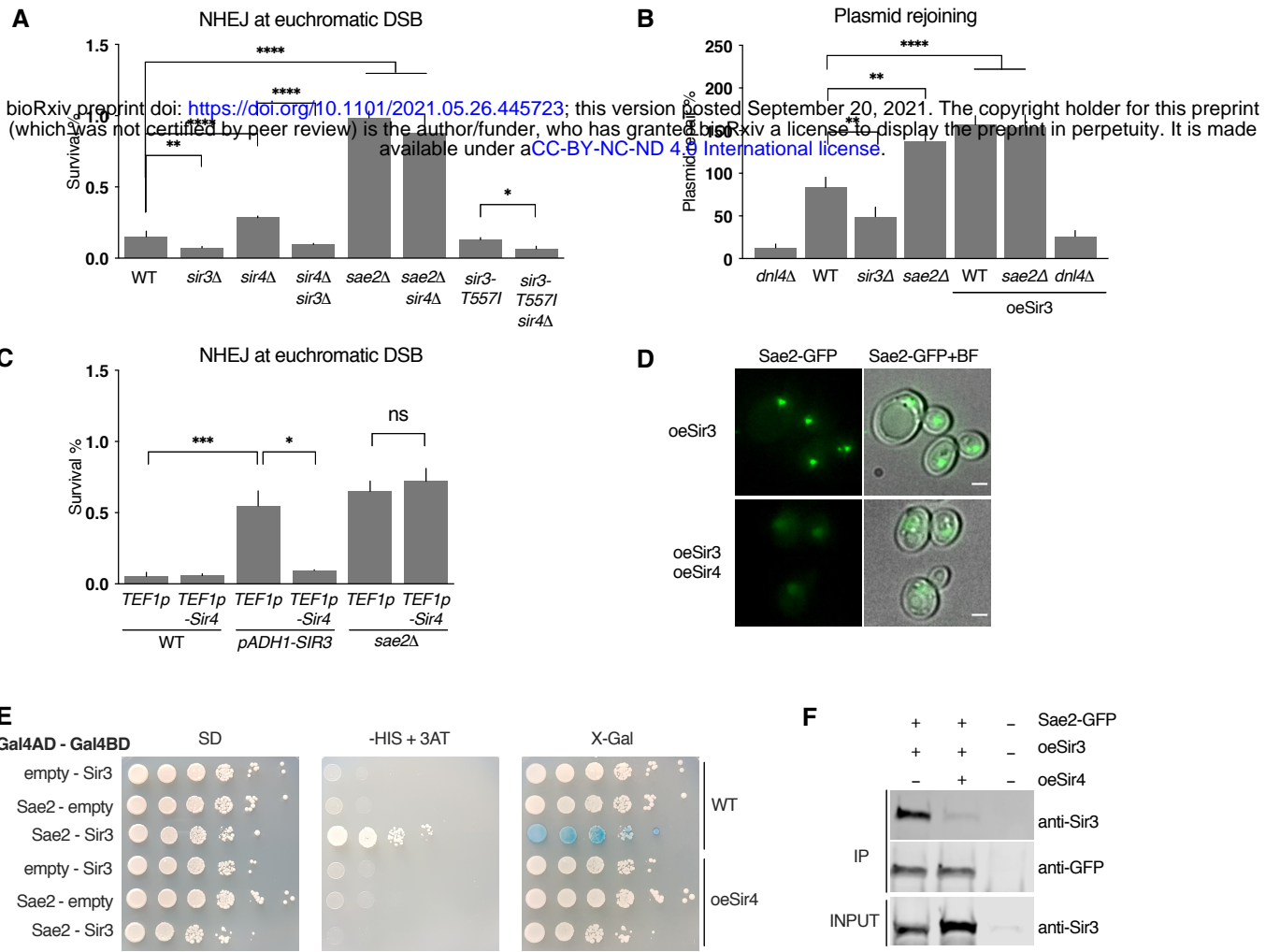


Figure 6

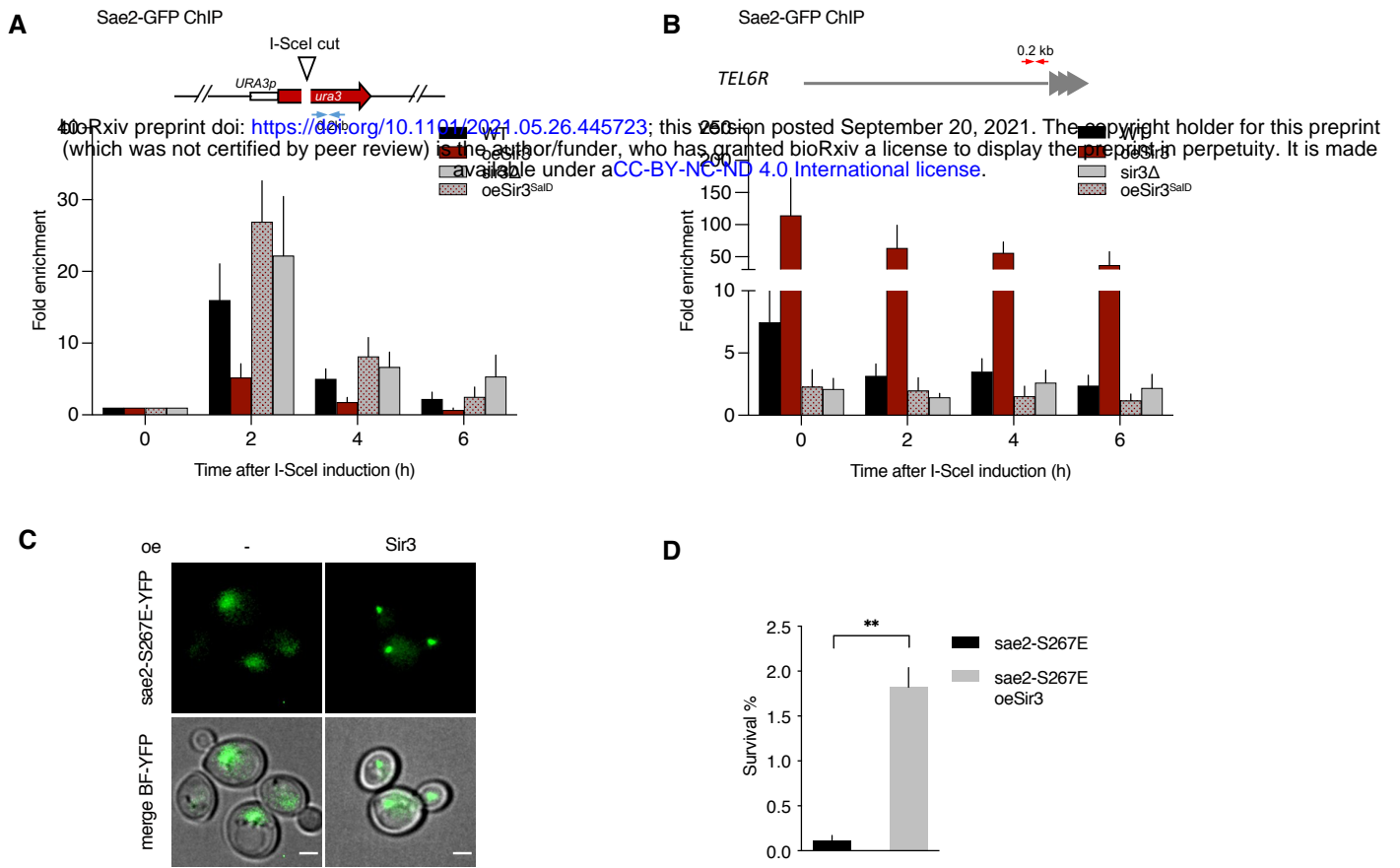
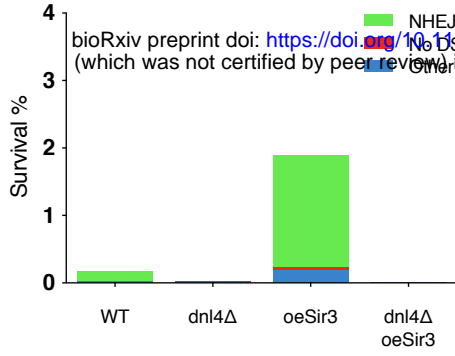
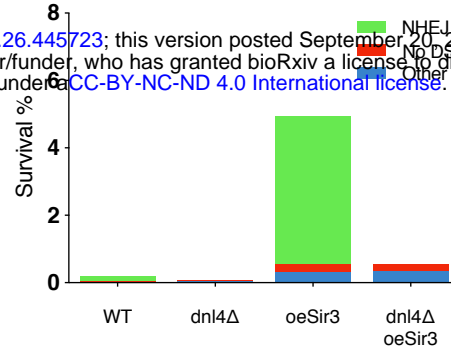
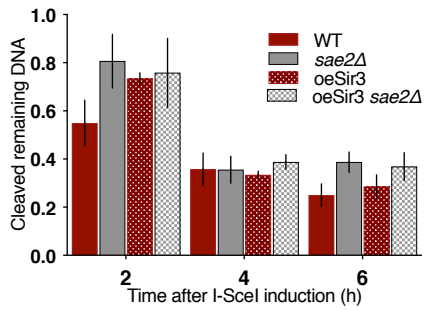
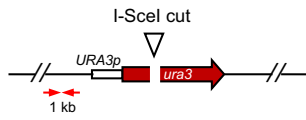
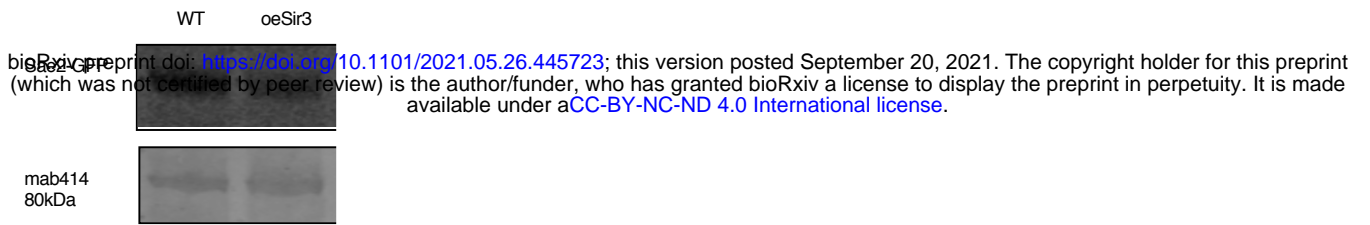


Figure 7

A**Euchromatic DSB****B****Heterochromatic DSB****C**



A

Sir3

BAH domain

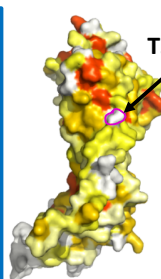
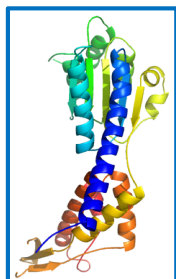
RBH Sir4 binding domain

WH domain



Multiple sequence alignment of Sir3 protein domains across various species including Saccharomyces cerevisiae, Aspergillus nidulans, and others. The alignment is divided into BAH, RBH, and WH domains. A specific region, Domain 531-723, is highlighted in a yellow box. A mutation T557 is indicated by a red asterisk in the RBH domain.

Xray structure
Sir3 (529-844)
PDB:3TE6



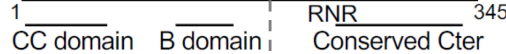
Conservation

531-723



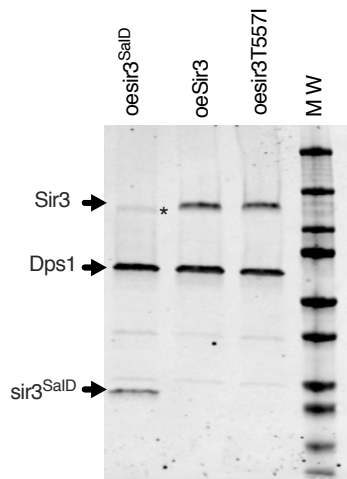
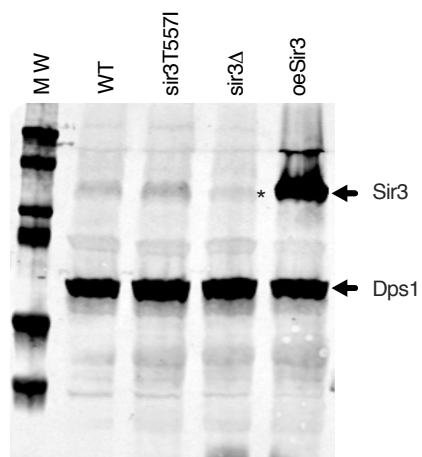
B

Sae2



Domain 173-345

Multiple sequence alignment of the Sae2 protein Domain 173-345 across various species. The alignment shows conserved residues and a mutation T557 is indicated by a red asterisk in the B domain.

A**B**

A